Thermal Science and Engineering Progress 55 (2024) 102955

Contents lists available at ScienceDirect

Thermal Science and Engineering Progress

journal homepage: www.sciencedirect.com/journal/thermal-science-and-engineering-progress

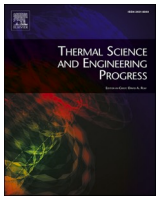

Material-level experimental study on utilising ionic liquid/graphene composites for sorption heat storage

Ahmed Rezk [a,b,1,*], Zoran Visak [c,1], Tahmid Hasan Rupam [d,1], James Hammerton [c,1], Qingchun Yuan [a,c,1], Matthew J. Derry [c,1], Bidyut Baran Saha [e,f,1]

[a] Energy and Bioproducts Research Institute (EBRI), College of Engineering and Physical Science, Aston University, Birmingham B4 7ET, United Kingdom
[b] Mechanical, Biomedical and Design Engineering Department (MBDE), College of Engineering and Physical Science, Aston University, Birmingham B4 7ET, United Kingdom
[c] Aston Advanced Material Research Institute, College of Engineering and Physical Science, Aston University, Birmingham B4 7ET, United Kingdom
[d] Department of Mechanical and Aerospace Engineering at the University of Missouri, Columbia, MO 65211, USA
[e] International Institute for Carbon-Neutral Energy Research (WPI-I2CNER), Kyushu University, 744 Motooka, Nishi-ku, Fukuoka-shi, Fukuoka 819-0395, Japan
[f] Mechanical Engineering Department, Kyushu University, 744 Motooka, Nishi-ku, Fukuoka-shi, Fukuoka 819-0395, Japan

ARTICLE INFO

Keywords:
Thermal Energy Storage
Composite sorbents graphene/ionic liquids
Water
Ethanol

ABSTRACT

Sorption heat storage technology has recently sparked an increasing interest because of its advanced heat storage capabilities. However, material-level heat and mass transfer challenges persist. This work contributes to the field by the development of new sorption composite materials that are comprised ionic liquids (1-ethyl-3-methylimidazolium methanesulfonate and 1-ethyl-3-methylimidazolium chloride) impregnated in 1–5 2D-layered graphene host matrix. Their sorption, heat transfer, heat storage, and charging/discharging rate properties were experimentally investigated using both water and ethanol as adsorbates. The adsorption isotherms and kinetics for both the adsorbates onto the developed composites and the parent ionic liquids were experimentally measured at different temperatures. The isosteric heat of adsorption for all the studied pairs was determined using the Clausius-Clapeyron method, showing an increasing trend with an increasing uptake. They showed that the specific heat storage capacity reached 187.5 kJ/kg when water was used as the working sorption agent. The corresponding heat charging/discharging rates are significantly higher, 69 %-78 %, than pure ionic liquids. Compared to silica gel as a baseline sorbent, ionic liquid-graphene composites' heat storage and transfer capacities are higher by three orders of magnitude. The thermal diffusivities of the developed composites were significantly higher than the baseline silica gel. These innovative sorption composites show great potential for improving thermal energy storage efficiency, making them suitable for applications in renewable energy systems, industrial processes, waste heat recovery, and climate control solutions. However, the developed composites achieved inferior performance compared to the silica gel baseline sorbent when using ethanol as a working fluid to utilise sub-zero ambient air as a heat source because of the relatively larger molecular size of ethanol.

1. Introduction

Heat is responsible for 50 % of the world's final energy consumption and 40 % of the CO_2 emission, which requires significant efforts to be decarbonised [1]. As such, thermal energy storage is crucial for sustainable heating that has gained an increasing interest because of its heat load-shifting capability by decoupling heat supply and demand [2]. It smooths the peak demand for heating, utilises the intermittency of renewable energy resources, maintains the operation of smaller heating equipment at peak efficiency conditions and recovers surplus thermal energy to promote energy saving via the heat network concept [3,4]. In this way, in typical dwellings, energy consumption was reduced by 67 % and CO_2 emission by 56 % [5]. Heat storage can operate interchangeably with electric energy storage to optimise renewable energy sources utilisation to achieve the highest possible conversion efficiency and to diversify future energy management. Because of its unique merits, there has been an increasing interest in sorption thermal energy storage in the last two decades [6,7]. Sorption-based heat storage is a subcategory of

* Corresponding author.
E-mail address: a.rezk@aston.ac.uk (A. Rezk).
[1] All authors contributed equally.

https://doi.org/10.1016/j.tsep.2024.102955
Received 14 February 2024; Received in revised form 29 August 2024; Accepted 30 September 2024
Available online 1 October 2024

thermochemical heat storage, which utilises a reversible physical process or chemical reaction involving a sorbent (e.g., silica gel, activated carbon or salt hydrate) and sorbate (e.g., water, ammonia or ethanol) to store a substantial quantity of heat in small volumes [8]. Applying heat dissociates the sorbent and sorbate, which are then stored separately. Bringing the sorbent and sorbate into contact again releases the sorption heat for use [9].

Sorption-based heat storages have unique advantages over others that are based on sensible and latent heat for its exceptionally high energy storing density (0.28 kWh/Litre), which is approximately ten times higher than the commercialised sensible heat storage (0.028 kWh/Litre) and two times higher than the emerging latent heat storage (0.14 kWh/Litre) [10,11]. Since the regenerated adsorbent and adsorbate are stored separately as sorption potential, sorption heat storage supports long, medium, and diurnal heat-storing virtually without degradation in the heat stored by heat losses [12–14]. The reaction between the sorbent and sorbate, physically or chemically, is usually associated with a heat pump effect that upgrades the heat to foster the effectiveness of thermal energy utilisation [15].

Reuse low-temperature renewable or waste heat in buildings is of specific importance for heating decarbonisation [16]. As such, sorption heat storage can employ a wide range of temperatures, including low-grade heat (below 200 °C), enabling the utilisation of various heat sources, such as geothermal, solar, and industrial low-grade waste forms [17]. Despite the advantages of sorption thermal energy storages, the poor material-level heat and mass transfer prolong the heat charging/discharging process and hamper their widespread utilisation [18]. Therefore, the effective implementation of sorption thermal management and storage depends on the development of sorbents with superior performance, as reported by Wu et al. [19].

Ionic liquids (ILs) have extremely low (practically null) volatility and excellent thermal stability over a wide range of temperatures [20]. Therefore, they are attractive to be used as alternatives for volatile organic solvents and components to form advanced materials. Because of their advanced thermophysical properties, the early use of ILs was for heat transport and phase change heat storage [21,22]. They are recently used to form highly thermally efficient nanofluid for heat transportation for solar energy application [23]. ILs showed a promising sorption potential as reported by Radakovitsch and Jess [24] that investigated the utilisation of [EMIM][$MeSO_3$]-coated silica gel for gases dehydration. ILs showed benefits for the sorption heat storage and transmission in addressing the shortcomings of conventional salt hydrates, such as lithium chloride, calcium chloride and strontium chloride hydrates [25–27]. Unlike salt hydrates, ILs have tuneable structures that can ultimately be tailored for optimal thermal storage by selecting their cations, anions, and the length of the alkyl chain in their cation to obtain the optimal sorption properties [28]. Therefore, they provide the potential to address the bottlenecking challenges in sorption heat storage, i.e., mass and heat transfer and the high corrosivity of salt hydrate sorbents.

Graphene is a single layer of carbon atoms arranged in a hexagonal structure. It can be synthesised from natural graphite ore by various exfoliation methods, chemical vapour deposition or graphene oxide reduction [29]. A single graphene layer exhibits a high thermal conductivity (3000–5000 W/mK) [29]. However, the thermal conductivity of graphene-based materials reduces as the number of carbon atomic layers increases. For example, reduced graphene platelets to over ten layers, commonly known as expandable graphite, showed bulk thermal conductivity between that for graphite and a single graphene layer, but closer to that for graphite [30]. Graphite ore is a 3D laminated graphene with a relatively high bulk anisotropic thermal conductivity of up to 1950 W/mK. It was also reported that acid treatment of graphite enhances its performance and thermal conductivity, which is most likely linked to better electron transfer after treatment [31].

Building on the advanced thermal properties of graphene derivatives, including graphite and its 2D variants, many researchers investigated their usage as parent adsorbents and host matrixes for salt hydrates in sorption systems [32]. Wang et al. [33,34] investigated the usage of expanded graphite and its treated variant with sulfuric acid as a host structure. They reported extraordinary thermal performance, but only after compacting it by exerting pressure up to 4 MPa. Although the exerted pressure enhanced the interlayer contact, hence the overall thermal conductivity closer to graphite ore, it significantly reduced the developed blocks' permeability, thus reducing the sorption kinetics. In addition, developing compressed host matrixes in blocks limits their application in the sorption reactor (adsorption bed) because of the reduced permeability. Kumar et al. [35] investigated the use of expandable graphite as a host matrix for $CaCl_2$ for thermal energy storage, which significantly enhanced the thermal response of the system. Grekova et al. [36] investigated using a multi-walled carbon nanotube (i.e., rolled graphene allotrope) as a host matrix for calcium chloride, lithium chloride and lithium bromide for sorption heat storage applications. The sorption performance of the developed composites showed promising results for the heat storage capacity, 1.7 kJ/kg and 1.6 kJ/kg, when using water and ethanol as sorbates, respectively. However, the implication of the developed composites' thermal performance was not investigated. Li et al. [37] utilised expandable graphite, a graphene variant, as a host matrix for LiOH and LiCl to develop highly stable sorbent composites that showed high level water sorption performance of up to 70 % for thermal energy storage application.

Ionic liquids have a strong potential to replace conventional salt hydrates in sorption heat storage, as mentioned above. However, utilising ionic liquids to develop sorption composites by impregnating them into host matrixes of advantageous thermal properties, such as graphene, and their *sorption heat storage* properties under realistic operating conditions are yet to be studied. Therefore, this study aims to address this important gap by experimentally investigating the development and utilisation of sorption composites comprising ionic liquids impregnated into a few-layered 2D graphene platelets host matrix in sorption heat storage applications. Two working fluids (i.e., sorbates), water and ethanol, were investigated to broaden the variety of the composite utilisation based on the ambient temperatures, where ethanol can operate under sub-zero or above-zero ambient while water can operate mostly under above-zero ambient. Therefore, the objectives of this study are (1) to develop ionic liquid/layered 2D graphene composites; (2) to determine the composites' heat transfer and sorption properties and benchmark them against the baseline silica gel; (3) to determine the material-level heat storage potential and the heat charging/discharging rate of the developed composites. The impact of successful attainment of these objectives is to enable harnessing the substantial water sorption capacities of the ILs within adsorption beds for practical applications in thermal energy storage. The GP as a host matrix, characterised by its elevated thermal diffusivity, can augment the thermal performance of ILs as adsorbent materials. By ensuring a homogeneous distribution of heat throughout the GP matrix, one can expect heightened rates for both charging and discharging processes, thus promising enhanced efficiency in thermal energy storage applications. Therefore, the key novelties of the present study are: (1) While most existing research utilised similar graphene-based material like GP as a thermal conductivity enhancer in composite adsorbents, this study is the first to employ GP as a host matrix to support ionic liquids sorbents; (2) This study emphasises developing a stable composite with high thermal diffusivity, ensuring complete containment of the ionic liquid within the host matrix under a broad operating conditions; (3) This study investigates ethanol as an adsorbate for sub-zero thermal energy storage applications.

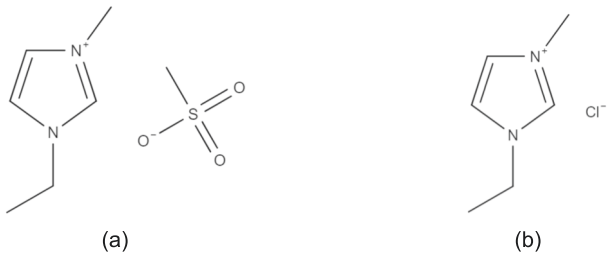

Fig. 1. Molecular view of (a) 1-ethyl-3-methylimidazolium methanesulfonate ([EMIM][CH_3SO_3]) and (b) 1-ehyl-3-methylimidazolium chloride ([EMIM][CL]).

Table 1
Experimentally measured mean physical properties of pristine few-layered graphene platelets (GP).

Matrix	Thermal diffusivity (mm^2/s)
GP	22.23
ExG	19.92
Graphite	4.92
GO	0.31
Silica gel	0.37

2. Materials and method

2.1. Materials

Two ionic liquids sourced from Sigma Aldrich UK: 1-ethyl-3-methylimidazolium methanesulfonate ([EMIM][CH_3SO_3]) and 1-ehyl-3-methylimidazolium chloride ([EMIM][Cl]), where their molecular view is shown in Fig. 1. Several graphene derivatives were employed and sourced from Graphitene Ltd in the UK: Graphene platelets of 1–5 layers (GP), Graphene oxide (GO) and expandable graphite (ExG). Graphite powder was sourced from Sigma Aldrich UK. Deionised water and ethanol were sourced from Fisher Scientific UK.

2.2. Composites preparation

The developed composites comprise ionic liquids and 1–5 2D graphene platelet layers (GP). ILs are emerging highly tuneable solvents of favourable thermal characteristics compared to the widely investigated salt hydrates, such as LiBr and LiCl. Unlike salt hydrates, ILs have low melting temperatures, which address the common crystallisation issue in composites comprising salt hydrates. It is noteworthy that crystallisation is one of the main reasons for the long-term instability of salt hydrate-based sorption composites, as it destroys the host matrix structure over time. ILs are non-volatile within a wide range of temperatures under which the heat storage operates, 35–75 °C for domestic use and above 100 °C for high temperature industrial applications. Although ILs might appear less commercially viable than metal salts counterparts, their widespread utilisation in applications like heat storage will promote their mass production; therefore, they might become more commercially viable in the long term.

GP was employed as a host matrix to develop the sorption composites. Its thermal diffusivity was determined experimentally and benchmarked against a baseline adsorbent silica gel (SG) and three widely known graphene derivatives: graphite, ExG and GO of 1–3 atomic layers. Table 1 shows the experimentally measured thermal diffusivity for GP, ExG, Graphite, GO and the baseline silica gel. It can be observed that GP is the most thermally diffusive at 22.23 mm^2/s. Interestingly, despite GO having fewer layers than GP and hypothetically showing high thermal performance, it showed the lowest thermal diffusivity value of 0.31 mm^2/s, even lower than that for silica gel. GO's low thermal diffusivity is attributed primarily to the interlayer oxygen particles, which increased the thermal resistance affecting the interlayer heat transfer [30]. Given that ExG is a graphene derivative of more layers (above 10 layers) than GP but less than graphite, it showed 19.92 mm^2/s thermal diffusivity. ExG's thermal diffusivity was higher than that for graphite of 4.92 mm^2/s of an extensively higher number of atomic layers but slightly lower than the GP counterpart.

The wet impregnation method was employed to develop the sorption composites because of its simplicity and ability to attain a high level of Interfacial and bulk deposition onto the host matrix surfaces. Ionic liquids were thoroughly degassed and cleaned from volatile solvents by applying a vacuum (0.1 Pa) at 60 °C before the use, following our established procedure [38]. Similarly, the host matrix was degassed at 150 °C for 12 h under a vacuum. First, aqueous solutions of each IL were prepared at IL concentrations of 10 – 40 wt%. As a result, the total aqueous solution exceeded that of the dried matrix (1 g host matrix to 25 g of the aqueous solution). Second, the dried host matrix was immersed into the aqueous solution and steered for 1 h to attain a homogenous host matrix/aqueous blend. Third, the developed mixture was left to rest for an hour to foster the impregnation of the host matrix. Finally, the excess solution was filtered, and the composite was dried gently at 150 °C for 1 hr. The preparation method is depicted in Fig. 2.

Initially, eight composites were developed, four from each IL [EMIM][CH_3SO_3] and [EMIM][Cl]. The composites are abbreviated as GP-Cl-x

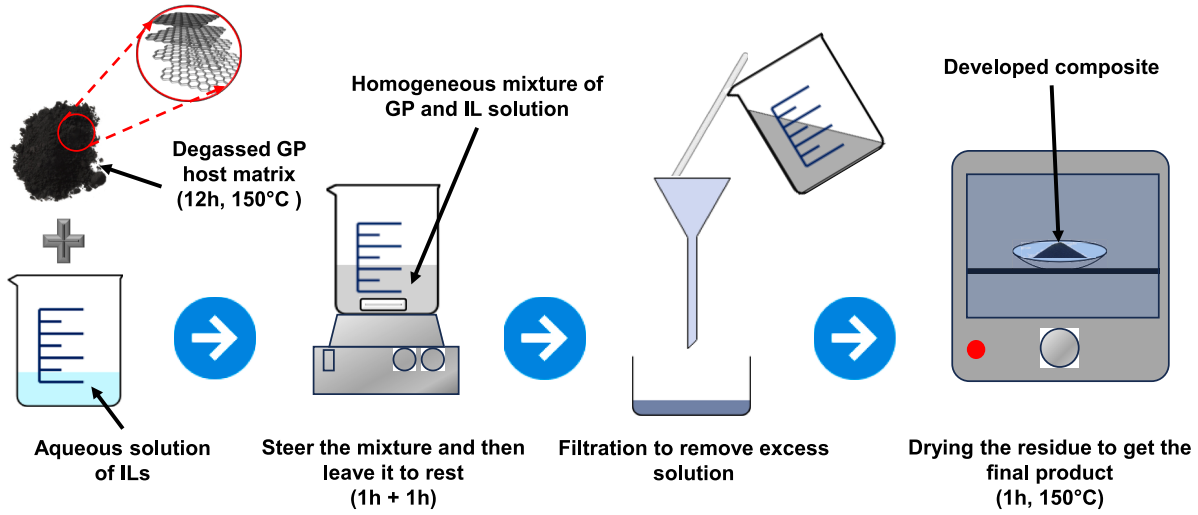

Fig. 2. Preparation procedure of the GP-IL composite adsorbents using the wet impregnation method.

Table 2
ILs content in the developed composites.

Composite	IL content (%wt)	Composite	IL content (%wt)
GP-Cl-10	31.0	GP-CH_3SO_3-10	38.4
GP-Cl-20	57.0	GP-CH_3SO_3-20	53.0
GP-Cl-30	65.5	GP-CH_3SO_3-30	64.9
GP-Cl-40	68.1	GP-CH_3SO_3-40	69.8

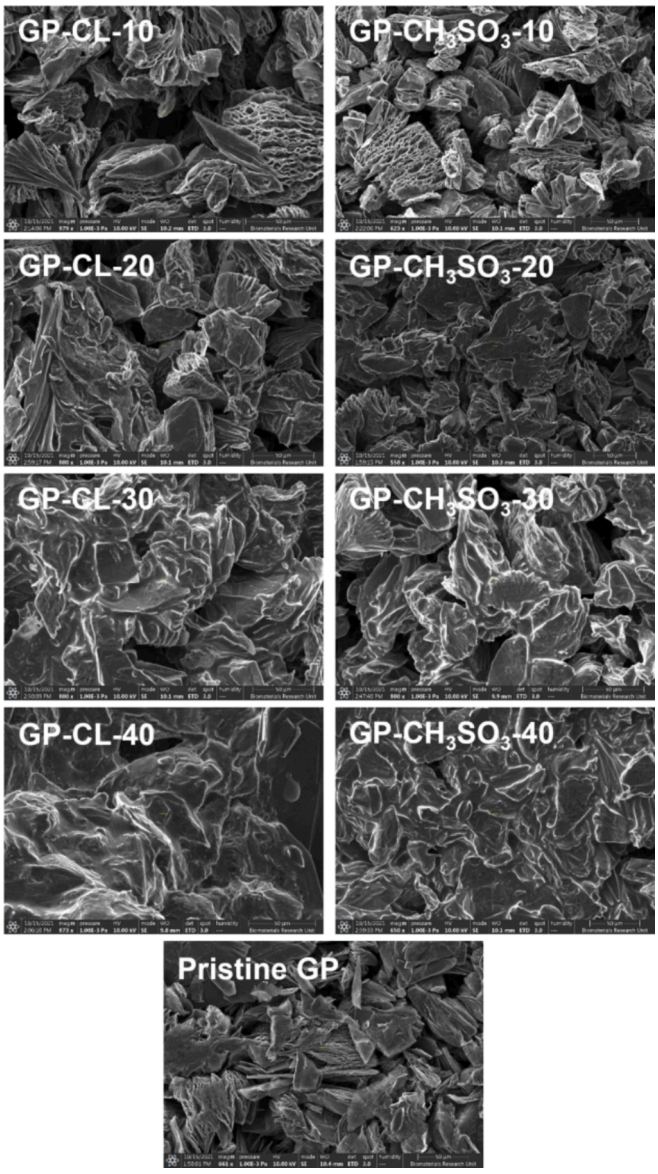

Fig. 3. SEM image of few-layered graphene derivative.

for these comprise [EMIM][Cl], and GP- CH_3SO_3-x for these comprise [EMIM][CH_3SO_3], where x denotes the %wt IL concentration of the utilised aqueous solution. Table 2 shows the final IL contents in the developed composites as measured by the TGA analyser and determined by Equation (1). It can be observed that the higher %wt IL concentration in the aqueous solution during the impregnation yielded composites with higher IL content; the IL content increment reduces as the aqueous solution's IL %wt concentration increases, showing the saturation of the host matrix.

$$ILcontent = \frac{mass_{IL}}{mass_{GP}} \times 100 \quad (1)$$

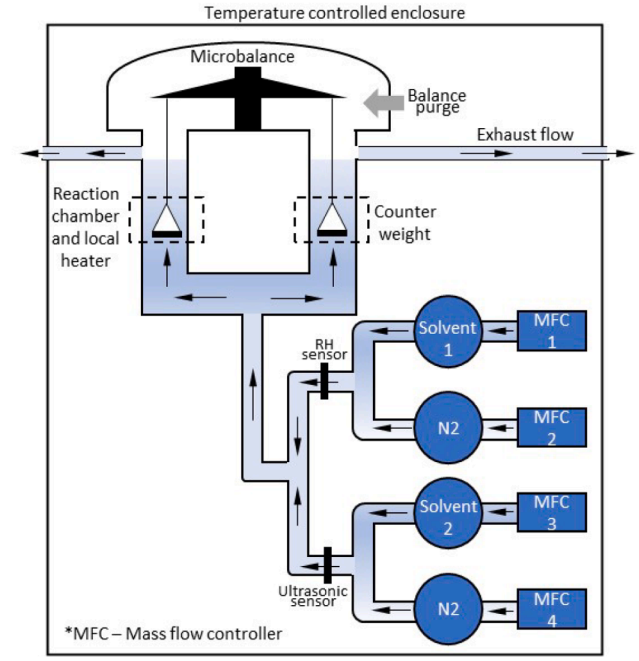

(a)

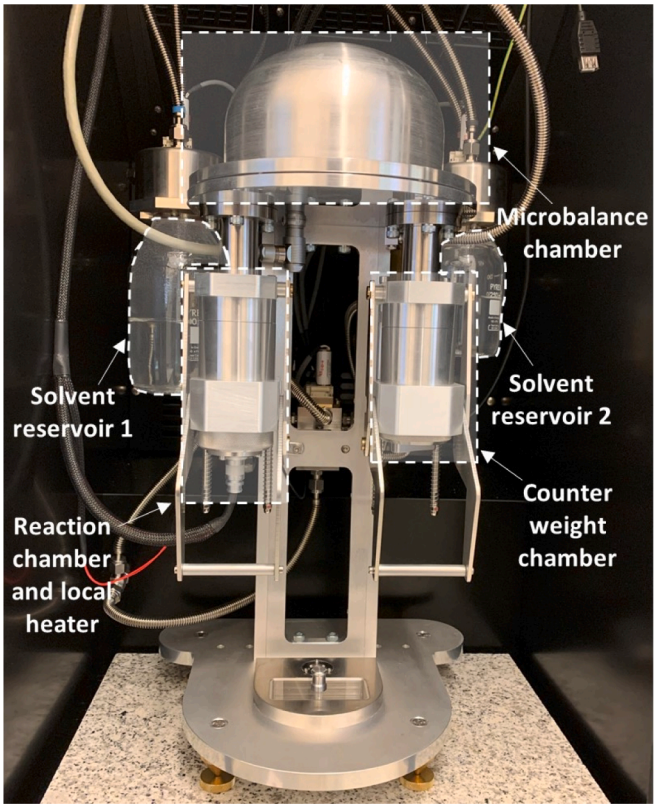

(b)

Fig. 4. Dynamic Vapor Sorption Analyser (DVS): (a) schematic diagram and (b) pictorial view.

Fig. 3 shows the SEM images of the developed composites. It can be observed that ILs are well-confined between the GP interlayer spacings for IL concentrations of 10–20 %wt. However, more precipitation on GP outside surfaces was observed for the ILs concentration of 30–40 %wt, which confirms the abovementioned host matrix saturation as expected

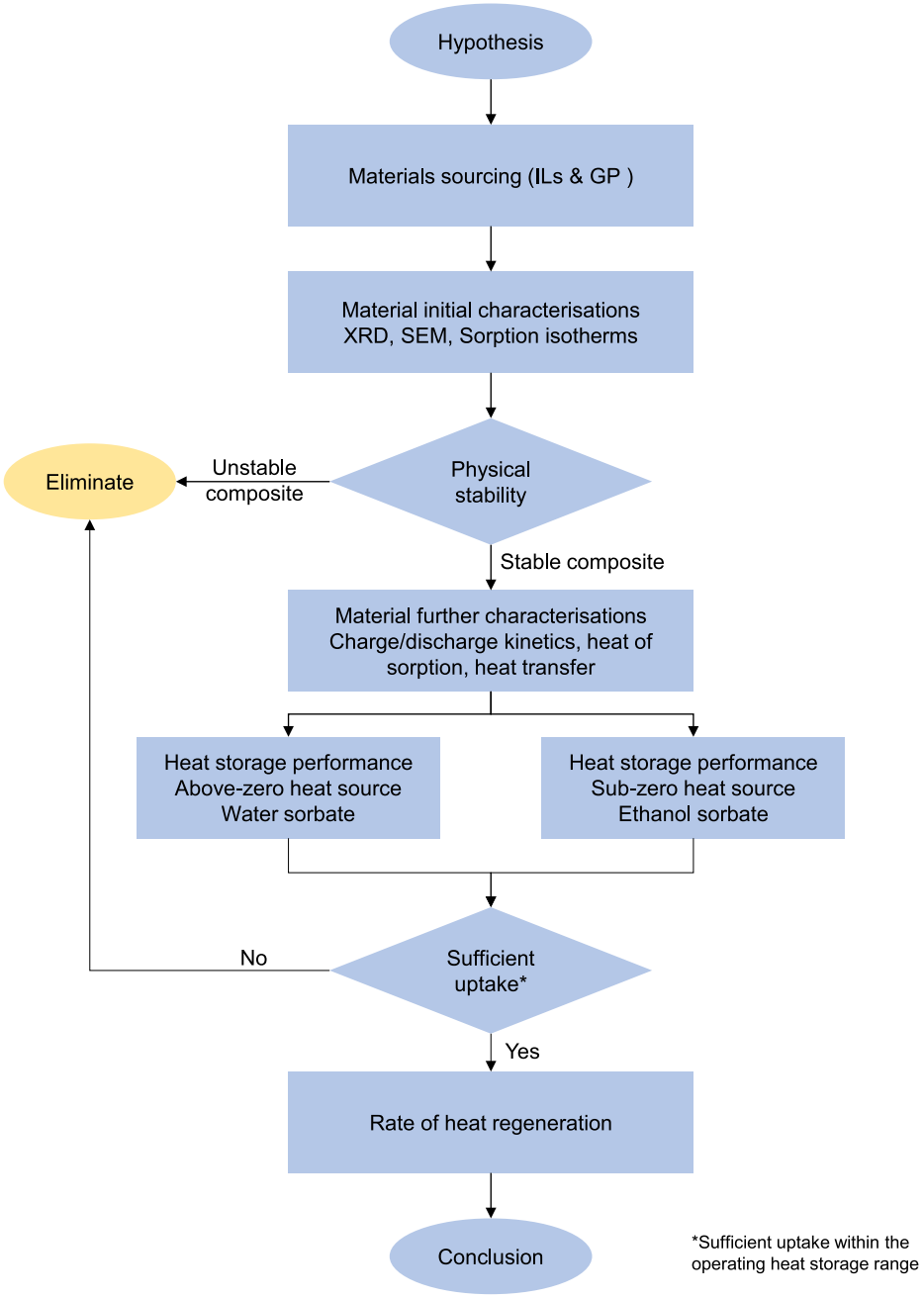

Fig. 5. Flow chart showing the research method.

from the IL content increment. Additional precipitation on the external surface increases the potential agglomeration sites on the host matrix's outside surface, showing the impracticality of utilising excessive IL concentration to develop the composite.

2.3. Experimental apparatuses

The sorption properties of the pure ILs and the developed composites were characterised using a dynamic vapour sorption analyser (DVS) gravimetric analyser, DVS Resolution™ by Surface Measurements Systems, as shown in Fig. 4. The sorption characteristics included adsorption isotherms, adsorption kinetics and imaging of the change in the physical appearance because of water and ethanol sorption/desorption. The apparatus is equipped with a mass balance and temperature resolutions of 0.01 μg and 0.01 °C, respectively. The partial pressure, P/P_0 resolutions were ± 0.1 %. at 25 °C and temperature stabilities are within ± 0.1 % and ± 0.05 °C over 6 hrs. Details about the equipment operation were previously reported by Rezk et al. [39].

The bulk thermal diffusivity was determined using a laser thermal diffusivity flash analyser (LFA) LFA467™ by NETZSCH. The same approach and similar apparatus were used by Pal et al. [40] and Banda et al. [41]. LFA comprises a laser source, a furnace to control the sample temperature, a sample holder, an infrared detector, and a data control unit. This apparatus has an accuracy and repeatability for thermal diffusivity measurement from 0.01 to 2000 mm^2s^{-1} ± 3 % and ± 2 % respectively at temperatures ranging from –100 °C to 500 °C. For each measurement, a laser pulse strikes the sample's front face, and the sample's adsorbed heat increases the rear face's temperature. Infrared detector determines the increase in the temperature, and the data control unit records the measured data. The data then is correlated to determine the thermal diffusivity of the sample. Experiments were

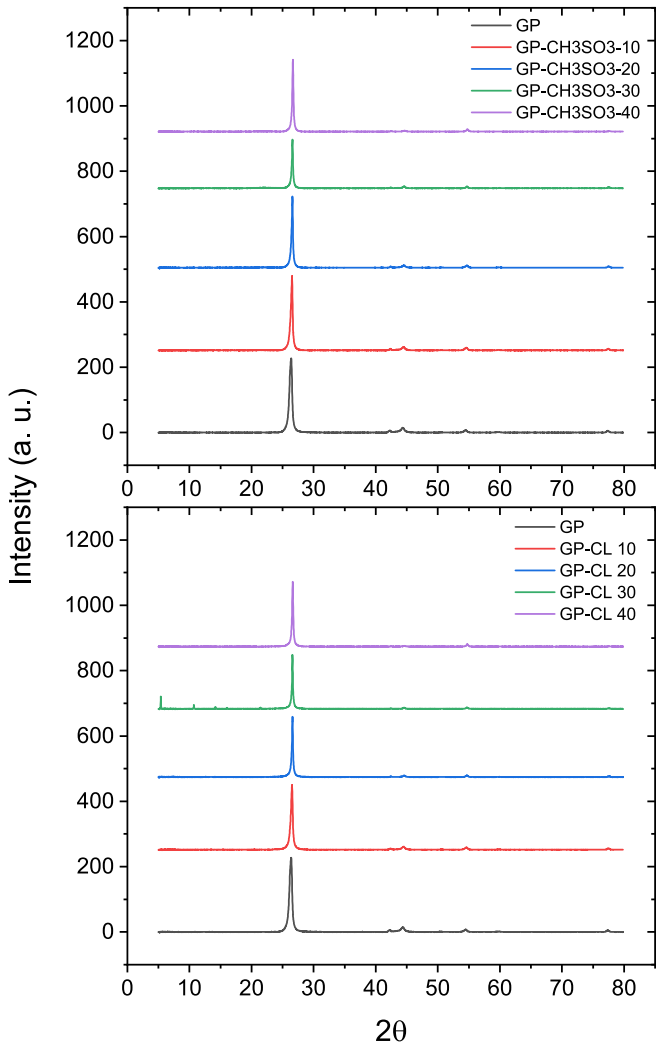

Fig. 6. XRD results of the developed composites.

undertaken three times with five laser shots at each trial. The results show close values with 0.01–0.02 standard deviation, giving a repeatability score of 0.005–0.01. The temperature rise at the sample's rear face was measured as a function of time to mathematically determine the thermal diffusivity (α) utilising Equation (2) by Parker et al. [42].

$$\propto = 0.1388\frac{l^2}{t_{05}} \tag{2}$$

where l is the thickness of the sample and t_{05} is the time required for the samples' rear face to reach half the maximum temperature. The apparatus's sample holder is round 12.7 mm in diameter and 1–3 mm thickness, which is within the apparatus's calibration range.

SEM imaging was employed to visualise and understand ionic liquid deposition's impact on the matrix. It enabled identifying precipitation of the ionic liquids on the external matrix's surface and the concentration of the excessive ionic liquid.

Powder X-ray diffraction (XRD) was recorded to understand the impact of ionic liquid impregnation on the host matrix structure of graphene. The XRD was performed on a Bruker D8 Advance operated at 40 kV and 40 mA using copper radiation ($\lambda_{CuK\alpha} = 1.54060$), with a 2θ range of 5–80° and a step size of 0.02°.

Thermogravimetric analysis (TGA) TGA8000™ by PerkinElmer was employed to determine each composite's final ionic liquid content. A nitrogen furnace purge of 40 mL/min applied to prevent oxidation or combustion of the sample during heating. Heating rate of 20 °C/min was used across the range of interest (200–400 °C for [EMIM][Cl], 200–550 °C for [EMIM][CH_3SO_3]). A final heating to 950 °C under an oxygen atmosphere was employed to ensure no inorganic residue was present in the sample. The experimental protocol of the study is illustrated in a form of a flowchart in Fig. 5.

3. Results and discussion

3.1. XRD assessment

Fig. 6 shows the XRD analysis of the ionic liquid/graphene composites is shown in. The diffractions show the characteristic pattern of graphite. The characteristic diffraction peaks of 002, 100 and 101, 004, 104 and 110 of graphite clearly appear in the GP and in every composite sample. This 002 peak is at $2\theta = 26.4°$ for the GP and shifts gradually and slightly towards $2\theta = 26.6°$, the peak for theoretical graphite structure as the IL impregnation amount increases. The characteristic peaks 100 and 101 are at $2\theta = 42.3°$ and 44.4° for the GP, respectively. After impregnating the ILs, the two peaks shift towards the values for the theoretical graphite structure: $2\theta = 42.4°$ and 44.6°. On the other hand, the two ILs at various concentrations always appear as amorphous at room temperature rather than as crystals under cryogenic conditions [43]. These small changes in the XRD diffraction angles imply that the impregnation of the ILs does not change the layered crystal structure of the GP but plays a role in driving the GP structure slightly towards perfection, probably, because of the thermal effect in the impregnation and drying processing.

3.2. Composites sorption properties

3.2.1. Sorption isotherms

Water and ethanol isotherms during sorption and desorption for the pure ILs ([EMIM][CH_3SO_3] and [EMIM][Cl]) and the developed composites were gravimetrically measured using the DVS apparatus to examine the influence of incorporated ILs into the GP host matrix, and the average water and ethanol uptake over the investigated pressure ratio range (0–90 %) were quantified, as shown in Fig. 7. The isotherm of [EMIM][CH_3SO_3] and [EMIM][Cl] and their composites with water are observed as Type II, given that the sorption is predominantly by the ILs into the 2D layered matrix [44]. Type-II isotherm is specific to the non-porous or microporous adsorbents, suggesting unrestricted monolayer-multilayer adsorption of the adsorbate molecules, which is completely reversible [45]. At a pressure ratio of approximately 10 %, highlighted in Fig. 7 a & b, the monolayer coverage is nearly completed, and the multilayer coverage is about to begin.

The isotherm of pure [EMIM][CH_3SO_3] and [EMIM][Cl] and their composites with ethanol are observed as type III, convex to the x-axis over the entire range, as shown in Fig. 7 c & d, indicating the multilayer sorption [46]. This type of isotherm shape indicates unrestricted multiplayer adsorption onto nonporous or microporous adsorbents. However, in this case, lateral interactions between the adsorbate materials dominate compared to the interactions between the adsorbent surface and the adsorbate molecule [45]. Besides, the investigated IL's affinity and their composites towards ethanol were relatively higher than their affinity towards water. For instance, the equilibrium ethanol uptake in pure [EMIM][CH_3SO_3] and [EMIM][Cl] was 30.6 % and 62.7 %, respectively, both of which are higher than the average water uptake. In addition, it can be observed that pure [EMIM][Cl] and its composites' affinity towards water and ethanol surpass those of [EMIM][CH_3SO_3] and its composites. For instance, the equilibrium water and ethanol uptake of pure [EMIM][Cl] was 13.3 % and 64.1 %, respectively, which are higher than pure [EMIM][CH_3SO_3].

The water and ethanol sorption isotherms for the investigated ILs and their composites were benchmarked against silica gel as a baseline sorbent. The isotherm curves show that the water equilibrium uptake of silica gel at relatively low pressure ratios outperformed that for GP-

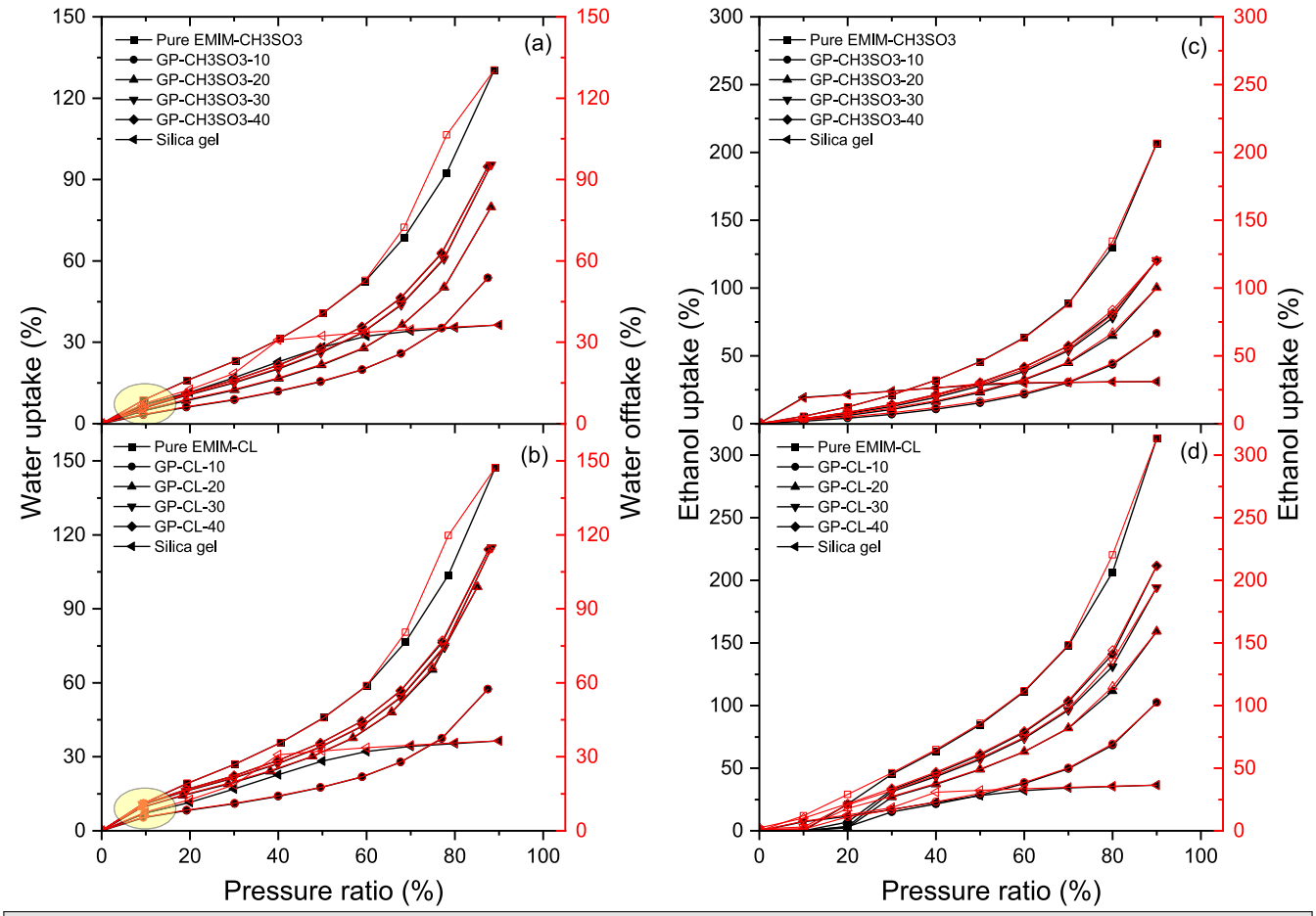

Average Equilibrium Uptake (kg/kg)											
Sorbate	EMIM-CH3SO3	GP-CH3SO3-10	GP-CH3SO3-20	GP-CH3SO3-30	GP-CH3SO3-40	EMIM-CL	GP-CL-10	GP-CL-20	GP-CL-30	GP-CL-40	Silica gel
Water	46.38	18.00	25.81	31.07	32.22	52.54	20.05	34.66	39.48	40.58	22.50
Ethanol	60.58	20.06	30.03	36.15	37.77	99.40	32.62	53.10	63.09	68.09	24.21

Fig. 7. Water and ethanol adsorption isotherms for the developed composites and Fuji silica gel benchmark at T=25 °C.

CH_3SO_3-(10–30) but underperformed GP-CH_3SO_3-40 and pure [EMIM][CH_3SO_3]. Silica gel showed a higher water equilibrium uptake at relatively low pressure ratios compared to GP-Cl-10, but a lower uptake compared to GP-Cl-(20–40) and pure [EMIM][Cl]. For relatively higher pressure ratios, the water adsorption of ILs and their composites outperformed that of silica gel. The pressure ratio at which the isotherms for silica gel intersect that for the developed composite varied based on the ILs content. Such an intersection occurred at a higher pressure ratio for lower IL content.

Silica gel/ethanol equilibrium uptake outperformed that for EMIM CH_3SO_3/ethanol and GP-CH_3SO_3-(10–40)/ethanol at pressure ratios below 50–70 %, varying with the IL content. However, silica gel/ethanol equilibrium uptake outperformed that for [EMIM][CH_3SO_3]/ethanol and GP-Cl-(20–30)/ethanol at relatively low pressure ratios, approximately 20 %, but conversely beyond that pressure ratio. For pressure ratios below nearly 40 %, GP-Cl-10/ethanol uptake underperformed that of silica gel/ethanol, but the opposite at higher pressure ratios. Higher IL content seemed more viable from the equilibrium uptake perspective. The gravimetric adsorption uptake was measured using the DVS analyser microbalance that was verified to have an accuracy of ± 0.05 μg by triplicated pre-experiment calibration, employing 100 mg mass. Figs. 8-10 also shows the cyclic stabilities of the samples where it depicts the repeatability of the experiments.

The equilibrium isotherms showed that increasing the IL content in the composite elevates the equilibrium uptake but the equilibrium uptake increment at IL concentration above 30 %wt becomes marginal, reflecting the marginal IL content increment because of the host matrix saturation. In addition, the SEM imaging showed better confinement of the ILs into the host matrix at relatively IL contents. The higher precipitation of ILs on the host matrix's outside surface with GP-Cl-40 and GP- CH_3SO_3-40 affects their practicality in the sorption bed. Therefore, the study focused on GP-Cl-(10–30) and GP- CH_3SO_3-(10–30). Although pure [EMIM][Cl] and their composites showed high affinity towards ethanol, they showed marginal sorption capacity within the heat storage operating range, corresponding to the pressure ratio of up to 20 %. Therefore, [EMIM][Cl]-(10–40)/ethanol pairs were eliminated from further investigation.

3.2.2. *Composites stability*

By alternating the pressure ratio between 0 % and 90 % for ten consecutive sorption/desorption cycles, the stability of the composites was experimentally investigated. The samples are depicted at the end of sorption and desorption to visualise the impact of the sorption/desorption processes on the ILs impregnation under such extreme operating conditions, as shown in Figs. 8-10. The gravimetric sorbate uptake over the time is shown on the lift and the composite pictorial views on the right in each of Figs. 8-10. None of the composites showed a visible loss of ethanol or water sorption capacity. GP-CH_3SO_3-(10–20) showed better IL confinement when operated under high water and ethanol concentration, i.e., high partial pressure of 90 %. However, for GP-

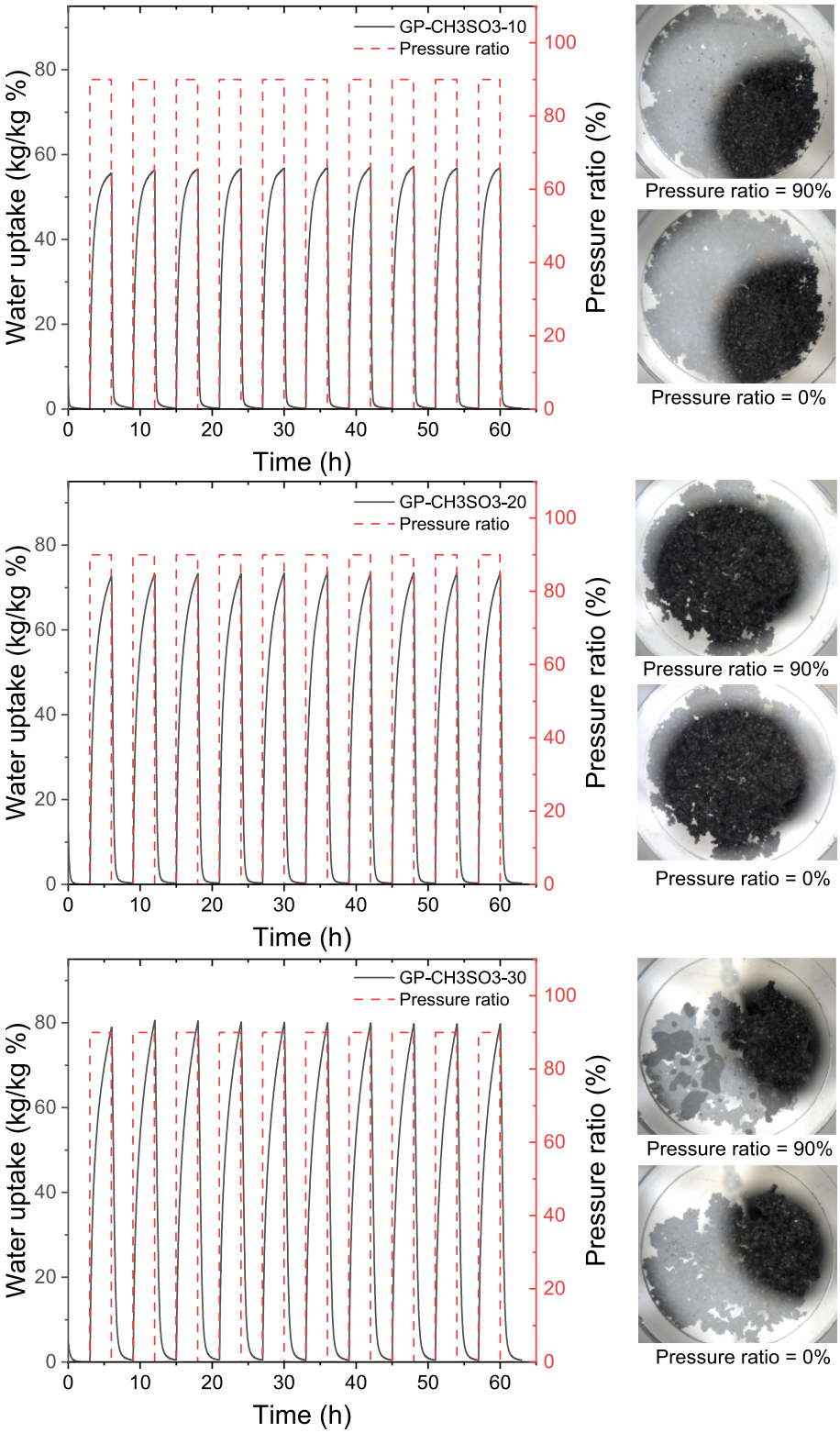

Fig. 8. Gravimetric water adsorption/desorption cycles for GP-CH_3SO_3-(10–30) (on the left) and the pictorial view of the composites (on the right) under 0–90% pressure ratios.

CH_3SO_3-30, the agglomeration effect was visible at such high partial pressure. For water sorbate, the agglomeration effect in GP-Cl-30 was more significant than GP-CH_3SO_3-30 because of the high hydrogen bond basicity (mainly anion-related) of chlorine anion-based ionic liquids [47] this anion is a very strong proton acceptor.

The agglomeration effect at high pressure ratio end, i.e., 90 % partial pressure, for GP-CH_3SO_3-30/ethanol was more profound than GP-CH_3SO_3-30/water. $CH_3SO_3^-$ anion has a higher attraction to ethanol than water because of the methanol group present in the anion, which allows for dispersive interactions besides hydrogen bonding. Agglomeration effects at elevated pressures can lead to the escape of ionic liquids (ILs) from the host matrix, potentially resulting in decreased adsorbate

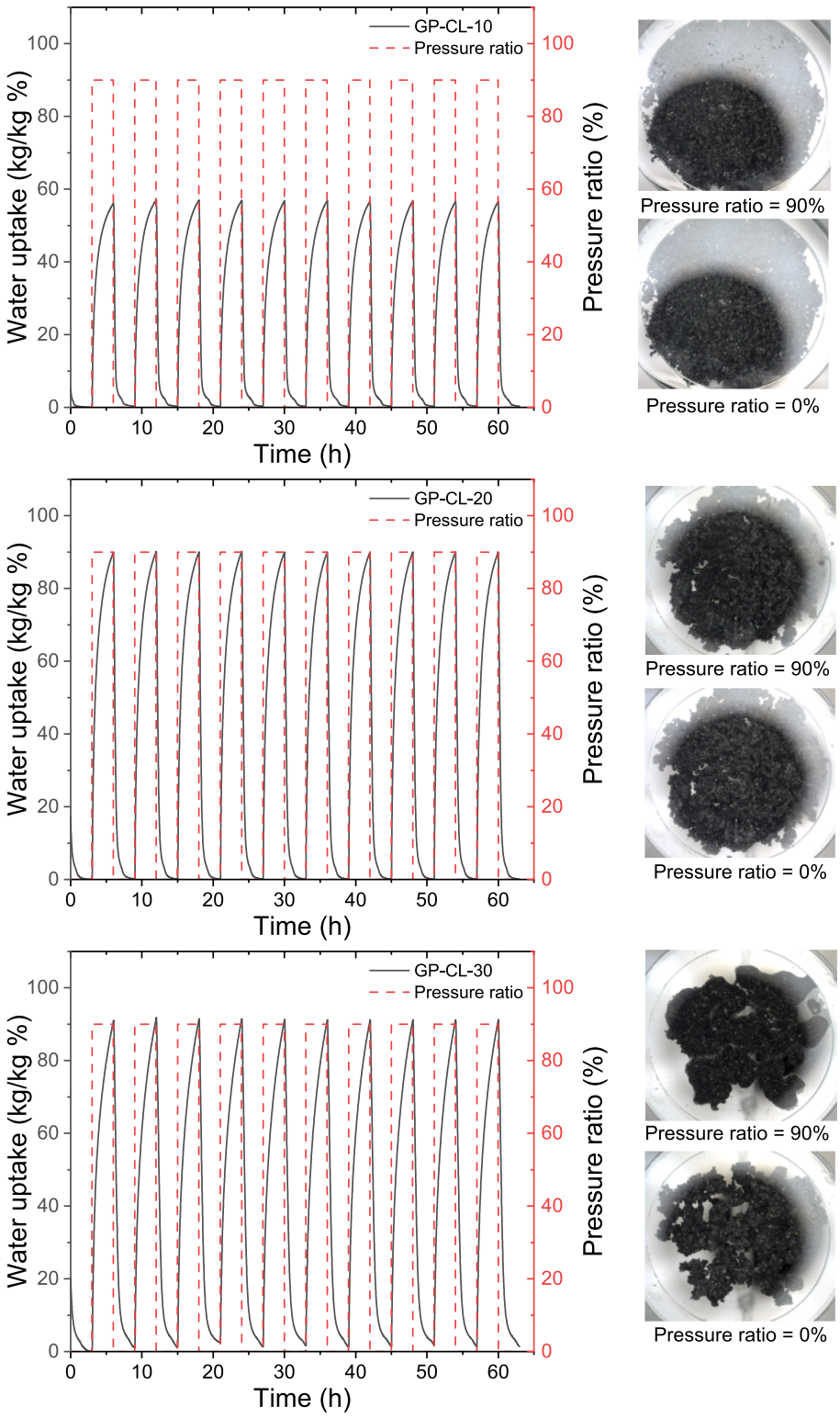

Fig. 9. Gravimetric water adsorption/desorption cycles for GP-Cl-(10–30) (on the left) and the pictorial view of the composites (on the right) under 0–90% pressure ratios.

uptake over multiple cycles. The ILs that escape will no longer be in contact with the heat exchanger surfaces or graphene nanoplatelets (GNPs), leading to reduced thermal performance because of the inherently low thermal diffusivity of ILs. However, despite the agglomeration occurring at high pressure ratios, it was not visible at pressure ratios equivalent to those corresponding to the practical cyclic operation of 20 % at the most, as depicted in Fig. 11, which will be thoroughly investigated at heat storage cyclic performance.

At a partial pressure of approximately 20 %, adsorption predominantly occurs at high-energy sites, resulting in releasing more heat because of the elevated adsorption enthalpy. When the partial pressures increase, additional adsorbate molecules shift towards lower energy sites, which decreases the adsorption enthalpy and consequently reduces heat release [48]. Therefore, it can be concluded that GP-CH_3SO_3-

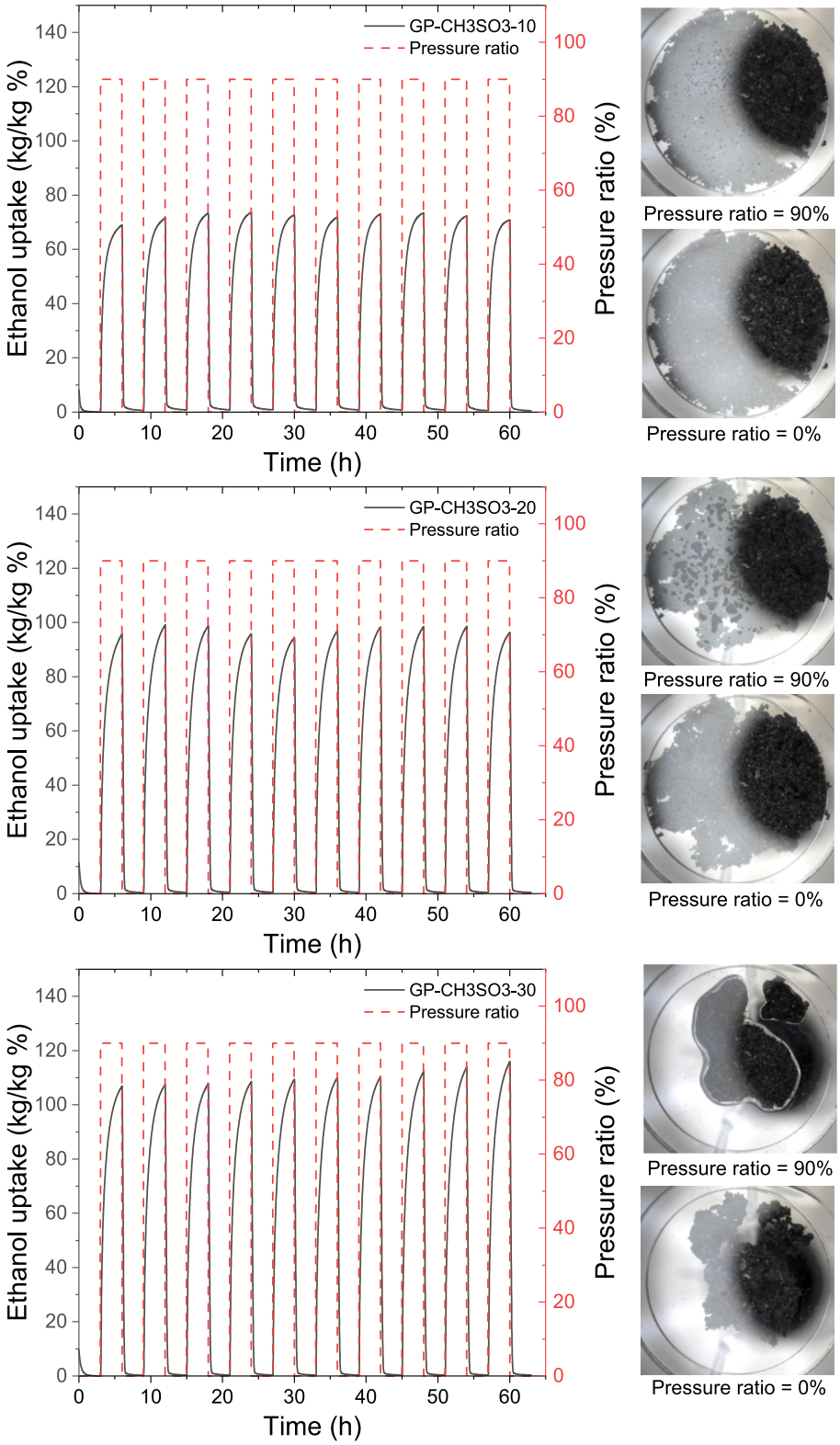

Fig. 10. Gravimetric ethanol adsorption/desorption cycles for GP-CH_3SO_3-(10–30) (on the left) and the pictorial view of the composites (on the right) under 0–90% pressure ratios.

30 and GP-Cl-30 are still practically viable, but further component-level experimental trials are required to develop more understanding from the practicality viewpoint.

3.2.3. *Heat of sorption*

The heat of sorption determines the exothermic/endothermic energies during the sorption/desorption per mole of the working fluid (i.e., water and ethanol) during their cyclic uptake/offtake. Therefore, the heat storage potential can be determined using Equation (3) by knowing

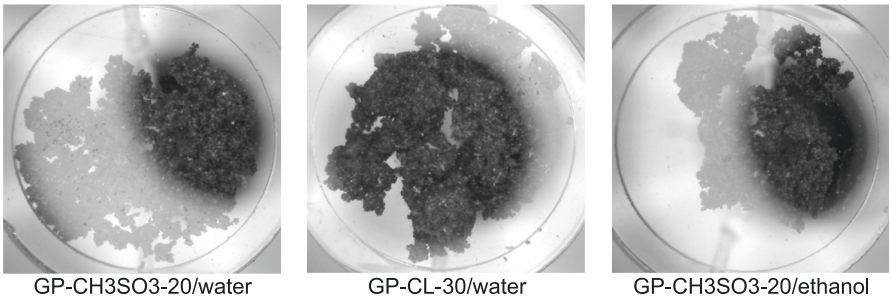

Fig. 11. Pictorial view of GP-Cl-30/water, GP-CH_3SO_3-20/water and GP-CH_3SO_3-20/ethanol at 20% partial pressure.

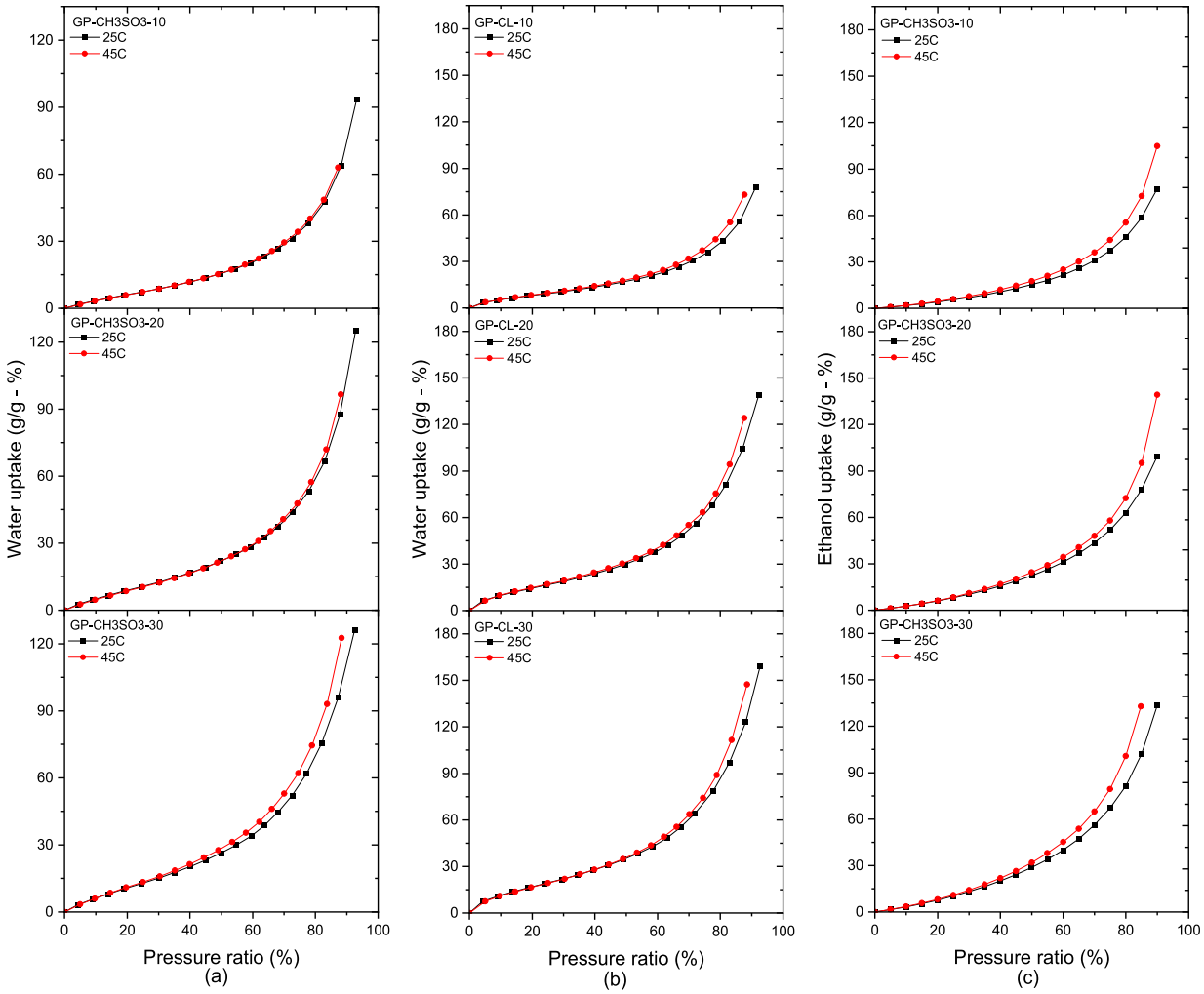

Fig. 12. Adsorption isotherms at 25C and 45C for (a) GP-CH_3SO_3/water (b) GP-Cl/water and (c) GP-CH_3SO_3/ethanol.

the heat of sorption.

$$q_{storage} = \frac{\Delta W \times E_a}{M} \tag{3}$$

where $q_{storage}$ is the heat storage per unit mass of the sorbent (J/ kg_{ads}); Δw is the cyclic water uptake (kg_{fluid}/kg_{ads}); E_a is the heat of sorption (J/mol); M is the molar mass (kg_{fluid}/mol) of the working fluid. The heat of sorption was determined using the Clausius-Clapeyron-type correlation given in its differential form in the Equation (4) [48,49], which also was previously presented by Rezk et al. in a simpler form given in Equation (5) [39]. The change in adsorbent mass measured the surface coverage because of the working fluid uptake. The Clausius-Clapeyron-type equation was solved by assuming entirely exothermic sorption at 10 points along the isotherms at two temperatures (T_1 = 25 °C and T_2 = 45 °C), and their corresponding pressure ratios $(P_{evap}/P_{ads})_1$ and $(P_{evap}/P_{ads})_2$ is shown in equations.

$$\frac{\partial ln(P/P_{bed})}{\partial T} = -\frac{E_a}{RT^2} \tag{4}$$

$$E_a = -R\frac{ln\left(\frac{(P/P_{bed})_1}{(P/P_{bed})_2}\right)}{\frac{1}{T_1}-\frac{1}{T_2}} \tag{5}$$

where R is the universal gas constant (J/mol.K).

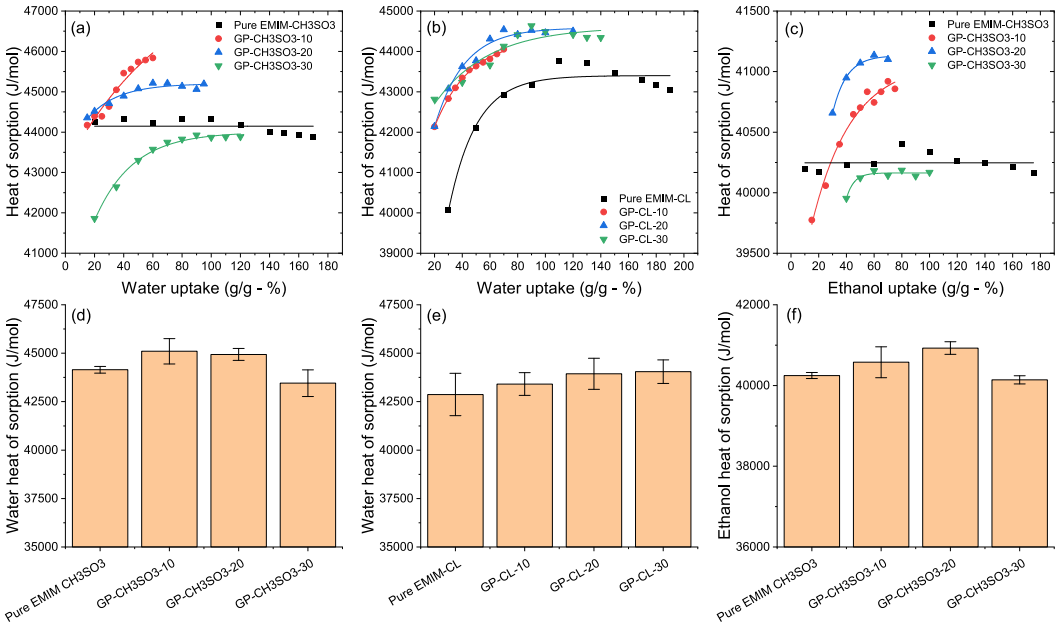

Fig. 13. The heat of sorption vs sorbate loading for (a) GP-CH_3SO_3(10–30)/water (b) GP-Cl(10–30)/water and (c) GP-CH_3SO_3(10–30)/ethanol; the average heat of sorption for (d) GP-CH_3SO_3(10–30)/water (e) GP-Cl(10–30)/water and (f) GP-CH_3SO_3(10–30)/ethanol.

The heat of sorption analysis was conducted for the sorption pairs: GP-CH_3SO_3-(10–30)/water, GP-Cl-(10–30)/water and GP-CH_3SO_3-(10–30)/ethanol. Fig. 12 shows the isotherms by which the heats of sorption were determined. It can be observed that the equilibrium sorption uptake increases by increasing the temperature, indicating the chemosorption of the developed composites, as ILs are the active sorption reagent in the developed composites [50].

The heat of sorption (E_a) at various loading, i.e., uptake, and their corresponding mean values are shown in Fig. 13. The E_a of water and ethanol for pure [EMIM][CH_3SO_3] are are observed to be nearly constant at 44,147 (±175) J/mol and 40,247 (±74) J/mol across the investigated range. The developed composites exhibited type II and type III isotherms with water and ethanol respectively, which alludes to the multilayer formation at relatively lower pressures. The multi-layers had more adsorbate molecules to interact among themselves and, because of this gas–gas interaction, the adsorption enthalpy showed an increasing trend with increasing uptake [51]. After the ionic liquid adsorbs adsorbate molecules via chemisorption, it undergoes expansion, which exposes high-energy active sites within the host matrix. This allows for the adsorption of additional adsorbate molecules at these high-energy sites, leading to an increase in adsorption enthalpy with increasing uptake. As these high-energy sites become depleted, the adsorbate gradually transitions to lower-energy sites within the host matrix, causing the adsorption enthalpy to plateau, followed by decreasing with further increase in the uptake. Incorporating [EMIM][CH_3SO_3] into the host matrix dispersed it and, therefore, increased the active sorption sites, leading to E_a trend increased by increasing the water loading. The E_a plateaued at water loading above 60 %, which was more distinguished for the relatively higher IL contents because of the high occupancy of the water vapour that reduced the degree of chemisorption. Given that pure IL is the active sorption reagent, the magnitude of E_a for the composites were, to an extent, around that of pure [EMIM][CH_3SO_3]. The E_a for GP-CH_3SO_3(10–30) showed almost the same trends. The plateaued heat of sorption at higher loading, occurring at higher partial pressure, aligns with the abovementioned molecules' shift towards lower energy sites accompanied by decreasing the adsorption enthalpy and the heat release [51].

The E_a of [EMIM][Cl] and its composites showed increasing trends by increasing the water loading. The effect of IL dispersion by intercalating [EMIM][Cl] is manifested by the less E_a change by increasing the water loading, meaning slightly enhanced chemisorption because the the increased sorption sites in the composite. Besides the slightly higher E_a for the developed composites compared to the pure IL. Averagely, the heat of sorption was 44,497 (±936) J/mol for GP-CH_3SO_3-(10–30)/water, 43,798 (±708) J/mol for GP-Cl-(10–30)/water, and 40,548 (±404) J/mol for GP-CH_3SO_3-(10–30)/ethanol.

3.3. Composite heat transfer properties

The thermal diffusivity of GP-CH_3SO_3-(10–30) and GP-Cl-(10–30) were experimentally determined using the LFA apparatus to assess the composites' heat transfer rate and benchmark them against the baseline adsorbent RD silica gel powder. Notably, the sample holder used to measure the thermal diffusivity of the developed composites and silica gel exerted a minimum pressure of 0.49 MPa to maintain consistent test conditions across the samples.

Fig. 14 shows the determined thermal diffusivities at different temperatures and their mean values. The thermal diffusivity was determined using five laser shots at each temperature, where the error bars show the standard deviation between 0.01 and 0.11 across the investigated range. The thermal diffusivity measurements as a function of temperature showed nearly constant values across all composites, including the benchmark silica gel. This stability in thermal diffusivity is because of the absence of any phase changes in the materials, which prevented significant deviations. Since thermal diffusivity is proportional to thermal conductivity and inversely proportional to specific heat capacity, the observed constancy suggests that in these composites, both thermal conductivity and specific heat capacity increased at similar rates with rising temperatures, resulting in stable thermal diffusivity. The ionic liquid within the composite has stable thermophysical properties over a broad temperature range. Unlike many other fluids, the specific heat and thermal conductivity of the ionic liquid do not change drastically with temperature, further contributing to the consistent thermal diffusivity. GPs are well known for their thermal stability across a wide temperature range, ensuring that the composite maintains steady thermal properties, leading to the observed constant thermal diffusivity.

Using silica gel as a baseline material, the deviation between the experimentally measured 0.37 mm^2/s and the reference value from the

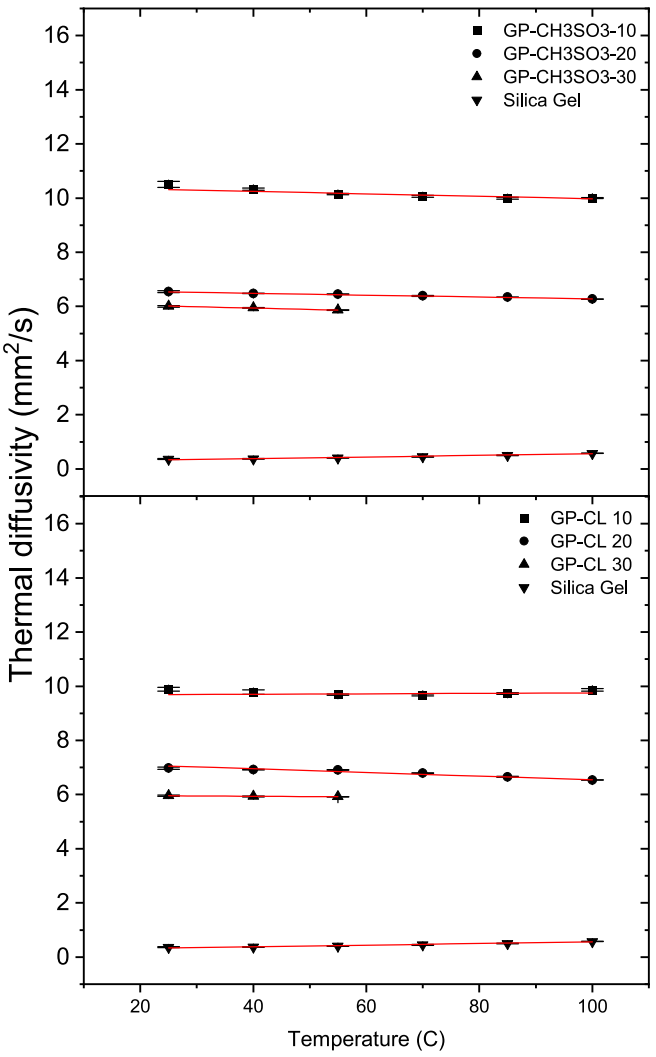

Average thermal Diffusivity (mm^2/s)			
GP-CH3SO3-10	10.18	*GP-CL-10*	9.77
GP-CH3SO3-20	6.41	*GP-CL-20*	6.8
GP-CH3SO3-30	5.94	*GP-CL-30*	5.95
Silica gel Exp	0.37	*Silica gel Ref*	0.31

Fig. 14. Temperature dependant thermal diffusivity of the developed composites: (a) GP/EMIM CH_3SO_3, and (b) GP/EMIM Cl composites.

literature is 19 %, which seems acceptable. The slightly higher thermal diffusivity of the experimentally measured thermal diffusivity for silica gel is attributed to its fine powder form and the applied pressure by the sample holder. However, insufficient information is available in the literature about the test conditions for those reported silica gel samples. It is also worth mentioning that the thermal diffusivity for GP-CH_3SO_3-30 and GP-Cl-30 stopped at 55 °C as these composites experienced IL leakage at higher temperatures because of the agglomeration effect. In practice, the composite might be packed, consolidated, or coated, and IL leakage in GP-CH_3SO_3-30 and GP-Cl-30 might not occur, as the composite compression is unlikely to be applied. Nevertheless, it highlights the need for further component-level experimental trials to investigate such a phenomenon.

It can be observed that, on the one hand, using GP as a host matrix enabled the development of sorption composites of high thermal diffusivity of an average of three orders of magnitudes higher than the conventional silica gel; on the other hand, increasing the IL content reduces the thermal diffusivity of the composites. For instance, the thermal diffusivity of GP-CH_3SO_3-10 is 58.8 % and 71.4 % than GP-CH_3SO_3-20 and GP-CH_3SO_3-30; the thermal diffusivity of GP-Cl-10 is 43.7 % and 64.2 % higher than GP-Cl-20 and GP-Cl-30. Changing the temperature showed marginal variation in the composites' thermal diffusivity, alluding to the stable thermal properties of the composites across the investigated temperature range.

3.4. Composites heat storage properties

Fig. 15 demonstrates the sorption heat storage's main components and operating principle. The operating conditions of the sorption heat storage are defined by four temperatures: (1) the charging temperature T_{ch}, (2) the heat sink temperature T_C, (3) the heat discharge temperature T_{dis} and (4) the evaporation, i.e., heat source, temperature T_e. During the charging mode, the heat at T_{ch} regenerates the sorbent during the desorption process, and the released working fluid is condensed by releasing its vaporisation heat to the heat sink at T_c. The charging heat can be surplus, or waste process heat, solar heat or heat obtained from the household boiler, electric heater, electric heat pump during off-peak operation. During the discharging mode, the dried adsorbent is re-exposed to the working fluid, and the sorption heat at T_{dis} is employed for, e.g., space heating, while the heat source at T_e drives the evaporator. The heat source could be ambient or underground heat, depending on the availability and the business case of the system installation. Although the underground heat source is virtually more feasible in cold climates because of its relatively higher temperature than the ambient that most likely falls below zero in winter seasons when heat storage is highly needed, e.g., Europe, it is more commercially demanding to establish and less short-term beneficial. However, other climates might require heat storage capacity but operate above zero ambient temperature, for example, South-West and South-East Asia, North Africa, and Central America, as reported by Grekova et al. [36]. The heat source temperature is crucial as the discharge heat utilised for, e.g., space heating, is a product of the sorption/evaporation process, where the heat source is the prime mover of such a process. The ambient predominantly acts as the heat sink for the condensation heat.

Fig. 16 shows the Clapeyron diagram for sorption heat charging/discharging cycles operating under two heat source propositions: above-zero evaporation (AZE) and sub-zero evaporation SZE. In AZE, the ambient temperature of 10 °C was considered as a heat source for the evaporator at 5 °C and heat sink for the condenser at 15 °C. In SZE, the ambient temperature of 0 °C was considered as a heat source for the evaporator at −5 °C and heat sink for the condenser at 5 °C. Given the low evaporative temperature of ethanol, it was investigated as a working fluid for AZE and SZE cycles. Utilising water as a working fluid operating at SZE is challenging; therefore, it was investigated under AZE operating conditions.

The DVS apparatus was employed to mimic the pressure ratios during the operation under AZE and SZE cycle, utilising ethanol and water as working fluids, as shown in Table 3. The pressure ratios are equivalent to P_{evap}/P_{ads} during heat discharging (i.e., adsorption) and P_{cond}/P_{des} during heat discharging (i.e., desorption) and temperatures to develop characteristic curves.

Fig. 17 shows pure [EMIM][Cl] and pure [EMIM][CH_3SO_3] and their composites under two consecutive heat charging/discharging cycles using the abovementioned heat storage operating conditions. The heat charging and discharging time were chosen as 180 min each in this study, where the investigated sorbents reached the equilibrium conditions. It was observed that the pure [EMIM][Cl] and pure [EMIM][CH_3SO_3] and their composites have a high affinity towards water, showing broader ranges of water uptake during the heat storage cycle. The sorption uptake/offtake rates during the heat storage cycle were faster for the developed composites than for the pure ionic liquids. It stemmed from dispersing the ionic liquids by intercalating them into the host matrix, increasing the composites' sorption sites. For instance, GP-CH_3SO_3-10 reached the maximum water cyclic uptake 69 % faster than

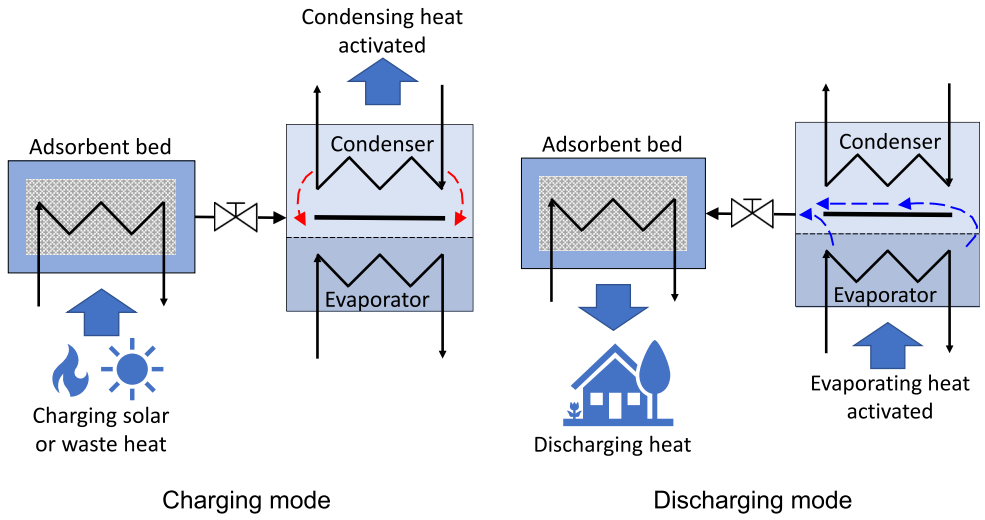

Fig. 15. Operating principle of sorption heat storage.

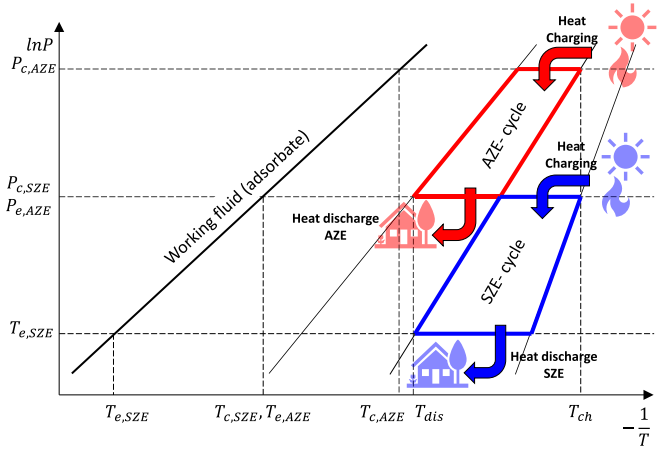

Fig. 16. Clapeyron diagram for the studied heat storage cycles.

Table 3
The operating temperature of the investigated heat storage cycles.

Cycle	T_{ch} [°C]	T_C [°C]	T_{dis} [°C]	T_e [°C]	T_{amb} [°C]
AZE	75	15	35	5	10
	Charging $(P_{des}/P_C)_{Water}$ = 4%		Discharging $(P_{ads}/P_e)_{Water}$ = 15%		
	$(P_{des}/P_C)_{Ethanol}$ = 5%		$(P_{ads}/P_e)_{Ethanol}$ = 16%		
SZE	75	5	35	−5	0
	Charging $(P_{des}/P_C)_{Ethanol}$ = 3%		Discharging $(P_{ads}/P_e)_{Ethanol}$ = 8%		

pure [EMIM][CH_3SO_3], and GP-Cl-10 reached the maximum water cyclic uptake 78 % faster than pure [EMIM][Cl].

Silica gel has a high affinity towards ethanol [39,52], leading to reversible fast sorption/desorption kinetics. In [EMIM][CH_3SO_3], the rate of ethanol offtake, i.e., charging, was 56 % faster than the rate of uptake, i.e., discharging, in AZE, and the rate of ethanol charging was 21 % faster than the rate of discharging in SZE. Like water sorption, the developed composites showed faster ethanol sorption kinetics than ILs. For instance, the GP-Cl-10 charging rate was 45 % and 85 % faster than pure [EMIM][CH_3SO_3] in AZE and SZE, and the discharging rate was 74 % and 84 % faster than pure [EMIM][CH_3SO_3] in AZE and SZE, respectively. These trends confirm that intercalating ILs into a few-layered graphene derivative promotes the heat charging/discharging rates by increasing the active sorption sites.

Fig. 18 shows the magnitude of net cyclic working fluid uptake and material-level heat storage per unit mass. By utilising water as a working fluid, it can be observed that the heat storage capacity of both ILs outperformed that of silica gel, while [EMIM][Cl]/water showed higher cyclic uptake and heat storage capacity than [EMIM][CH_3SO_3]/water, as chlorine anion, has very high hydrogen basicity. The developed composites showed less cyclic water uptake and heat storage compared to the ILs, which increases by increasing the ILs concentration. Therefore, the larger magnitude of ILs per unit mass of the composite fosters the heat storage capacity. Only GP-Cl-(20–30) outperformed the baseline silica gel sorbent among the developed composites. Considering the magnitude of heat storage and the charging/discharging rates, GP-Cl-30 seemed the most suitable composite that outperformed the baseline silica gel for water sorption. The storage density of 187.47 kJ/kg GP-Cl-30 might not seem that high when compared to the commonly studied salt-impregnated composite adsorbents' energy densities such as for silica gel/$CaCl_2$ (1080 kJ/kg), zeolite H–Y/$MgCl_2$ (970 kJ/kg), SBA–15/$Al_2(SO_4)_3$ (334 kJ/kg), MCM–41/$Al_2(SO_4)_3$ (612 kJ/kg) [53–55]. However, it is noteworthy that the salts utilised in such high energy density composites are highly corrosive, especially when working at high temperatures, and their composites are not free from delinquency effect and the inefficient long-term stability resulting from host matrix deficiency because of the crystallisation. Most importantly, the tunability of ILs makes them promising materials for further research on designing them for specific use, e.g., thermal energy storage.

Utilising ethanol as a working fluid with [EMIM][CH_3SO_3] and its composites showed similar trends as water working fluid. Despite the high affinity of silica gel towards ethanol, the net cyclic ethanol uptake is hindered by the ethanol molecules trapped in silica gel micropores, as ethanol molecules, for comparison, are nearly 30 % larger than water molecules, as reported by Rezk et al. [39]. The restricted physical mobility of ethanol molecules caused, for example, silica gel/ethanol uptake to swing between 16.4 % and 19.0 % when operating under the AZE cycle compared to a broader range of 4.2 % – 10.1 % in silica gel/water.

[EMIM][CH_3SO_3] showed 161 % and 134 % higher cyclic ethanol uptake and heat storage than silica gel in the AZE cycle. However, the SZE cycle showed 28 % and 20 % less cyclic ethanol uptake and heat storage than silica gel. The smaller cyclic uptake range was primarily because of the smaller range of pressure ratio swing in the heat charging/discharging cycle located in the isotherm profile region of small ethanol uptake of up to 5.4 % kg_w/kg_{ads} for [EMIM][CH_3SO_3] (type III) but 19.3 % kg_w/kg_{ads} for silica gel (type I). Accordingly, silica

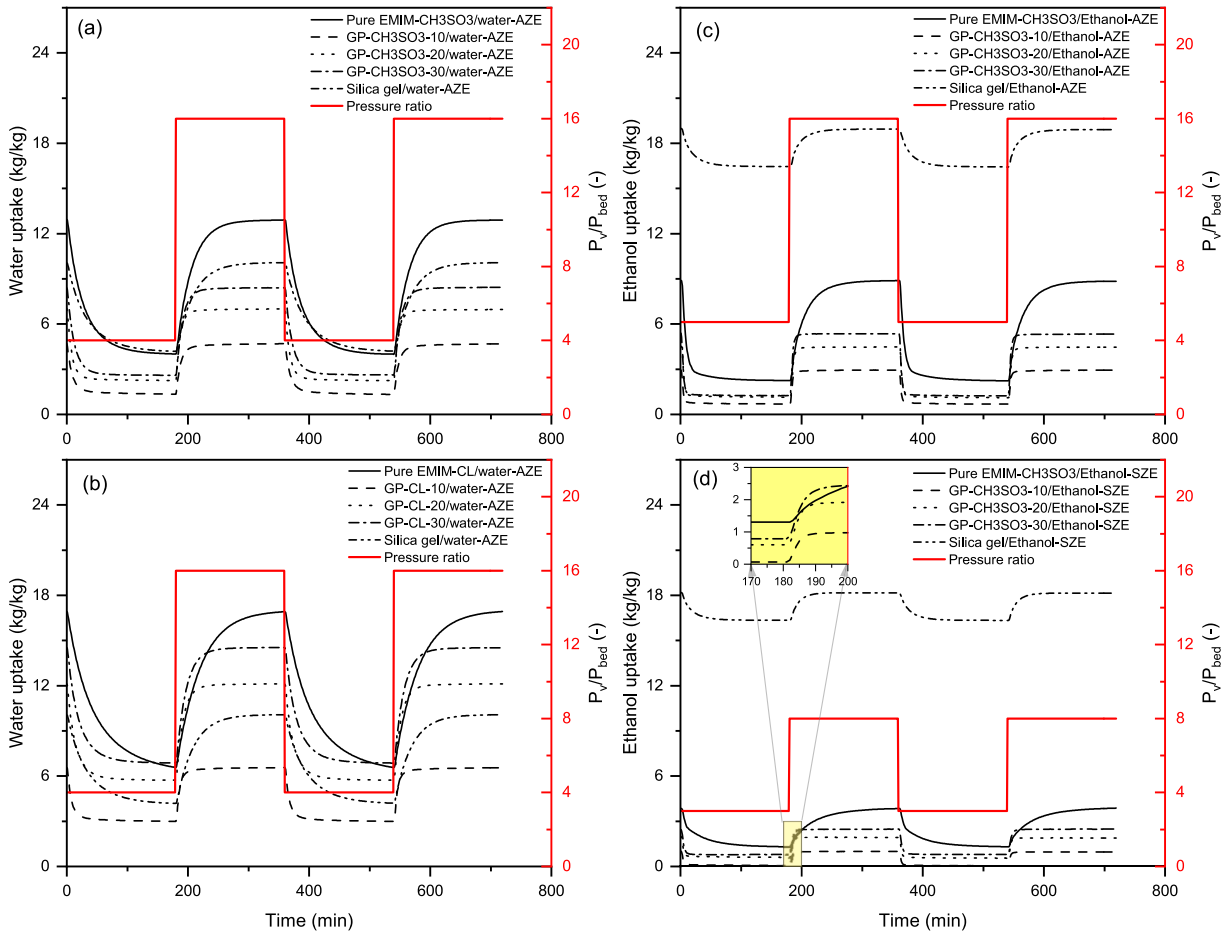

Fig. 17. Heat charging / discharging cycles using water sorbate and $T_{charge} = 75\ ^{\circ}C$; $T_{cond} = 15\ ^{\circ}C$; $T_{evap} = 5\ ^{\circ}C$; $T_{dcharge} = 35\ ^{\circ}C$ (a) time frame uptake profile; (b) net cyclic uptake.

gel appears more feasible for the SZE sorption heat storage cycle, despite the limited uptake range results from the ethanol molecules size concerning the high porosity of silica gel, which can be addressed by developing silica gel with more accessible sites to ethanol, i.e., large porosity structure. Nevertheless, developing a porous structure of larger pore sizes will compromise the overall surface area.

Emphasising AZE, where [EMIM][CH_3SO_3] outperforms the baseline silica gel, GP-CH_3SO_3-20 and GP-CH_3SO_3-30 showed sorption heat storage per unit mass 22 % and 46 % higher than silica gel. However, GP-CH_3SO_3-10 showed sorption heat storage per unit mass 20 % less than silica gel in this instance, primarily because of the relatively low IL content. Therefore, emphasising AZE, GP-Cl-30/water remains the optimal choice within the investigated material.

3.5. Composites' thermal regeneration properties

Fig. 19 shows the materials' response during the charging process at 75 °C by utilising local heating elements in the DVS apparatus and water as a working fluid. It can be observed that the silica gel showed the slowest response to the charging heat, followed by the ILs: [EMIM][CH_3SO_3] and [EMIM][Cl]. The developed composites showed the fastest charging rates, but the magnitude of the water offtake plateau varied depending on the magnitude of IL contents. No significant variation in the charging rate was observed for the developed composites, revealing the denomination of the high thermal diffusivity for the host matrix in promoting the charging process. It manifests the high thermal diffusivity of the developed composites and its implication on the charging rate, i.e., heat capture. It also demonstrates the benefit of using ILs of a favourable thermal response.

The developed composites exhibit excellent adsorption properties and thermal energy storage capacity. However, certain factors must be considered if integrated into a heat exchanger. The composites can be applied as flakes or powder through spray or dip coating using a binder on the heat exchanger surfaces [56]. Alternatively, consolidated composites can be fabricated for insertion between the heat exchanger fins [57]. It should be noted that impregnating the composites with ILs beyond 30 % presents challenges in developing stable composites, which could lead to performance issues as a result of IL leakage at higher vapour pressures. These practical implications highlight the complexity and versatility of implementing these materials into thermal energy storage systems. Further research is needed in this area, which is of significant interest.

4. Conclusion and prospects

4.1. Conclusion

This article presents an experimental study of newly developed sorption composites of ILs intercalated into few-layered graphene. The composites were experimentally investigated for their sorption heat storage properties using water and ethanol as working fluids. Two groups of composites were developed using different ILs, namely [EMIM][CH_3SO_3] and [EMIM][Cl]. The findings show promising potential for these composites, as listed below.

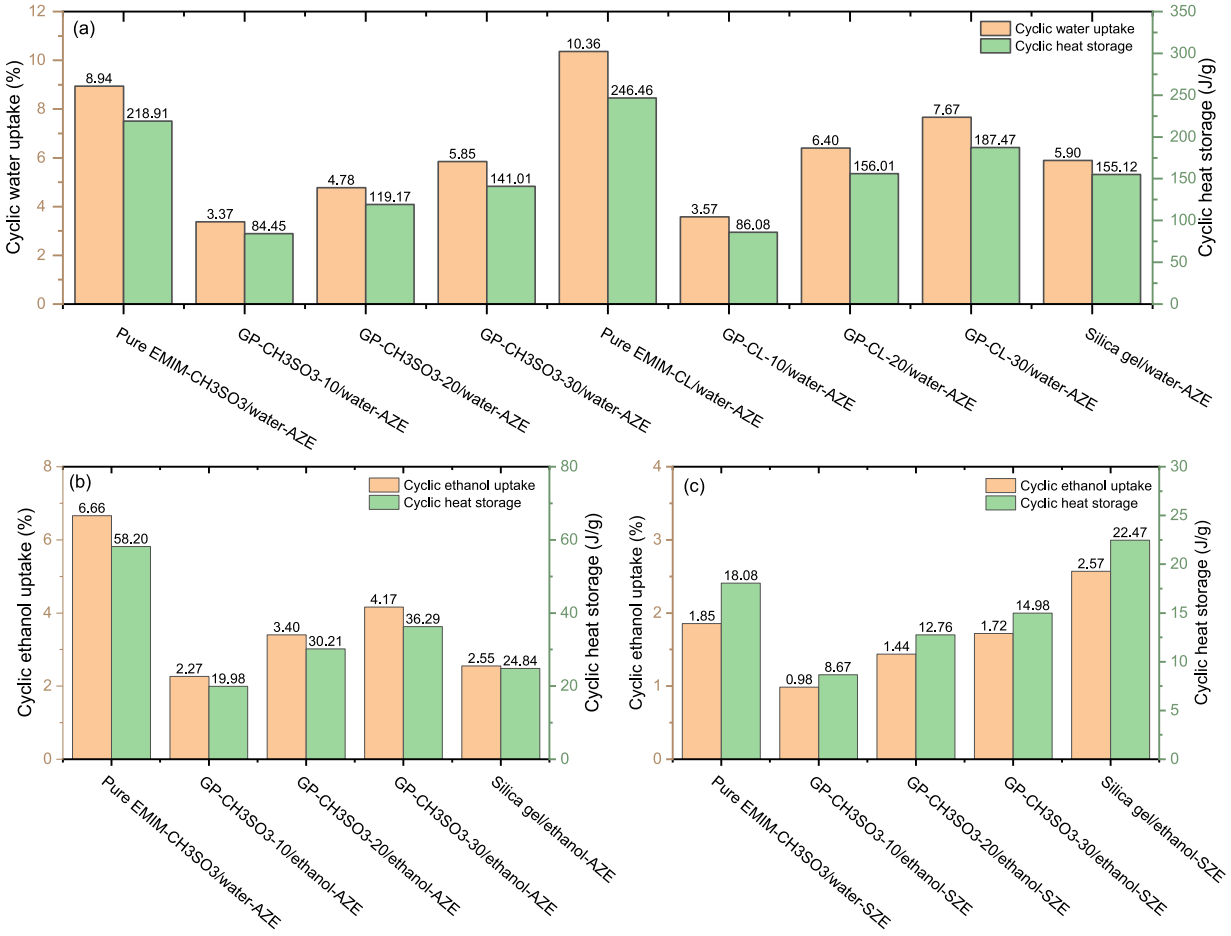

Fig. 18. Cyclic heat storage capacity using water and ethanol sorbates under AZE and SZE operating conditions.

- The developed composites were chemically stable for utilising water and ethanol sorbates. However, high IL contents developed from utilising aqueous solutions above 30 %wt during the impregnation led to a high agglomeration level of ILs/ethanol and ILs/water outside the hosting matrix. Therefore, composites of lower IL content appear more practically viable.
- GP-Cl-x and GP-CH_3SO_3-x had high chemosorption levels for water (type II isotherms) and ethanol (type III isotherms), which increases with increasing IL concentrations. However, [EMIM][Cl]-x/ethanol pairs had low sorption uptake at vapour pressures ratio < 20 %.
- The IL dispersion into the host matrix promoted the chemosorption effect due to increased active sorption sites, fostering the benefits of employing a few-layered graphene matrix.
- The developed composites were of exceptionally high thermal diffusivity, reaching three orders of magnitude higher than the conventional silica gel. The high thermal diffusivity significantly promoted the sorption heat charging rate.
- The GP-ILs composite has a high heat storage potential, with GP-Cl-30 being the most suitable and better than the baseline silica gel for water sorption. However, because of low ethanol uptake, GP-CH_3SO_3-x/ethanol did not show viable heat storage potential under SZE.

4.2. Prospects

Although the material level investigation confirms the developed composite's high sorption heat storage potential, more investigation is required to understand their performance at the component and system levels. In addition, the advanced heat transfer performance of the host matrix and the advanced sorption performance of ILs, along with being highly tuneable, can be leveraged to design composites that achieve high levels of sorption heat storage at fast charging/discharging rates.

CRediT authorship contribution statement

Ahmed Rezk: Writing – review & editing, Writing – original draft, Supervision, Resources, Project administration, Investigation, Funding acquisition, Formal analysis, Conceptualization. **Zoran Visak:** Writing – review & editing, Writing – original draft, Supervision, Resources, Investigation, Funding acquisition, Formal analysis, Conceptualization. **Tahmid Hasan Rupam:** Writing – review & editing, Writing – original draft, Investigation, Formal analysis. **James Hammerton:** Writing – review & editing, Writing – original draft, Investigation, Formal analysis. **Qingchun Yuan:** Writing – review & editing, Writing – original draft, Visualization, Validation, Investigation, Formal analysis, Data curation. **Matthew J. Derry:** Writing – review & editing, Writing – original draft, Investigation, Formal analysis. **Bidyut Baran Saha:** Writing – review & editing, Writing – original draft, Methodology, Investigation, Funding acquisition.

Declaration of competing interest

The authors declare the following financial interests/personal relationships which may be considered as potential competing interests: Ahmed Rezk reports equipment, drugs, or supplies was provided by The Royal Society. Ahmed Rezk has patent pending to GB2207186.4. Zoran Visak has patent pending to GB2207186.4. No other activities or relationships that cause a conflict of interest.

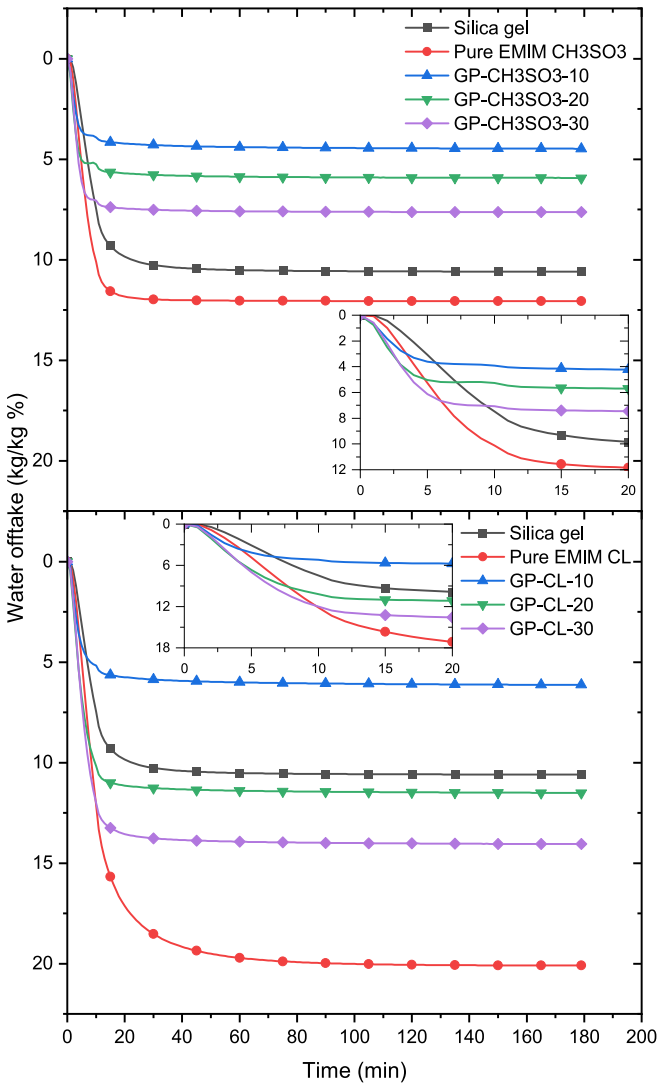

Fig. 19. The rate of composite regeneration 75 °C heat source.

Data availability

Data will be made available on request.

Acknowledgement

This work was supported in by The Royal Society (grant no. IES\R3 \203128).

References

[1] M. Thonon, et al., Simultaneous charging and discharging processes in latent heat thermal energy storage: a review, Thermal Science and Engineering Progress 47 (2024) 102299.
[2] M.A. Hayat, et al., Enhancing thermal energy storage in buildings with novel functionalised MWCNTs-enhanced phase change materials: towards efficient and stable solutions, Thermal Science and Engineering Progress 47 (2024) 102313.
[3] M.H. Nguyen, et al., Thermochemical sorption heat storage: Investigate the heat released from activated carbon beads used as porous host matrix for MgSO4 salt, J. Storage Mater. 59 (2023) 106452.
[4] J. Che, et al., Modeling of energy carrier in solar-driven calcium-looping for thermochemical energy storage: heat-mass transfer, chemical reaction and stress response, Chem. Eng. J. 463 (2023) 142435.
[5] J.P. Da Cunha, P. Eames, Compact latent heat storage decarbonisation potential for domestic hot water and space heating applications in the UK, Appl. Therm. Eng. 134 (2018) 396–406.
[6] Y. Zhang, R. Wang, Sorption thermal energy storage: Concept, process, applications and perspectives, Energy Storage Mater. 27 (2020) 352–369.
[7] W. Li, et al., Salt hydrate–based gas-solid thermochemical energy storage: current progress, challenges, and perspectives, Renew. Sustain. Energy Rev. 154 (2022) 111846.
[8] D. Aydin, S.P. Casey, S. Riffat, The latest advancements on thermochemical heat storage systems, Renew. Sustain. Energy Rev. 41 (2015) 356–367.
[9] J. Sunku Prasad, et al., A critical review of high-temperature reversible thermochemical energy storage systems, Appl. Energy 254 (2019) 113733.
[10] D. Lefebvre, F.H. Tezel, A review of energy storage technologies with a focus on adsorption thermal energy storage processes for heating applications, Renew. Sustain. Energy Rev. 67 (2017) 116–125.
[11] Y.C. Lin, et al., Performance analysis on open thermochemical sorption heat storage from a real mass transfer perspective, J. Storage Mater. 54 (2022) 105267.
[12] D. Mahon, et al., Feasibility study of MgSO4 + zeolite based composite thermochemical energy stores charged by vacuum flat plate solar thermal collectors for seasonal thermal energy storage, Renew. Energy 145 (2020) 1799–1807.
[13] A. Krönauer, et al., Mobile sorption heat storage in industrial waste heat recovery, Energy Procedia 73 (2015) 272–280.
[14] A. Crespo, et al., Optimizing the discharge process of a seasonal sorption storage system by means of design and control approach, J. Storage Mater. 60 (2023) 106652.
[15] S. Vasta, et al., Adsorption heat storage: state-of-the-art and future perspectives, Nanomaterials (Basel, Switzerland) 8 (7) (2018) 522.
[16] E. Cihan, et al., Entropy analysis and thermal energy storage performance of PCM in honeycomb structure: effects of materials and dimensions, Thermal Science and Engineering Progress 38 (2023) 101668.
[17] H. Schreiber, F. Lanzerath, A. Bardow, Predicting performance of adsorption thermal energy storage: from experiments to validated dynamic models, Appl. Therm. Eng. 141 (2018) 548–557.
[18] B. Han, A. Chakraborty, Functionalization, protonation and ligand extension on MIL-53 (Al) MOFs to boost water adsorption and thermal energy storage for heat transformations, Chem. Eng. J. 472 (2023) 145137.
[19] S.-F. Wu, et al., Solar-driven dual-mode cascading cycle based on ammonia complexation reaction for flexible seasonal thermal management, Chem. Eng. J. 452 (2023) 139536.
[20] A.E. Visser, N.J. Bridges, R.D. Rogers, Ionic Liquids: Science and Applications, American Chemical Society, Washington, DC, USA, 2012, p. 2012.
[21] J. Yang, et al., Novel ionic liquid crystals based on N-alkylcaprolactam as cations, Chem. Mater. 19 (10) (2007) 2544–2550.
[22] L. Moens, et al., Advanced Thermal Storage Fluids for Solar Parabolic Trough Systems. In ASME Solar 2002: International Solar Energy Conference, 2002.
[23] L. Das, et al., Improved thermophysical characteristics of a new class of ionic liquid + diethylene glycol/Al2O3 + CuO based ionanofluid as a coolant media for hybrid PV/T system, Thermal Science and Engineering Progress 36 (2022) 101518.
[24] F.R. Radakovitsch, A. Jess, Gas dehydration using the ionic liquid [EMIM][MeSO3] supported on silica gel – structural and water vapor sorption properties, Chem. Eng. J. 398 (2020) 124689.
[25] M. Gaeini, et al., Characterization of microencapsulated and impregnated porous host materials based on calcium chloride for thermochemical energy storage, Appl. Energy 212 (2018) 1165–1177.
[26] M.M. Tokarev, et al., Novel ammonia sorbents "porous matrix modified by active salt" for adsorptive heat transformation: 2. Calcium chloride in ACF felt, Appl. Therm. Eng. 30 (8) (2010) 845–849.
[27] L. Jiang, et al., Investigation on heat and mass transfer performance of novel composite strontium chloride for sorption reactors, Appl. Therm. Eng. 121 (2017) 410–418.
[28] A. Mehrkesh, A.T. Karunanithi, Optimal design of ionic liquids for thermal energy storage, Comput. Chem. Eng. 93 (2016) 402–412.
[29] M. Anju, N.K. Renuka, Graphene–dye hybrid optical sensors, Nano-Structures & Nano-Objects 17 (2019) 194–217.
[30] N.K. Mahanta, A.R. Abramson, Thermal conductivity of graphene and graphene oxide nanoplatelets. In 13th InterSociety Conference on Thermal and Thermomechanical Phenomena in Electronic Systems, 2012.
[31] S. Shakeel, A.H. Anwer, M.Z. Khan, Nitric acid treated graphite granular cathode for microbial electro reduction of carbon dioxide to acetate, J. Clean. Prod. 269 (2020) 122391.
[32] A.S. Alsaman, et al., 2D materials for adsorption desalination applications: a state of the art, Thermal Science and Engineering Progress (2024) 102455.
[33] L.W. Wang, et al., Thermal conductivity and permeability of consolidated expanded natural graphite treated with sulphuric acid, Carbon 49 (14) (2011) 4812–4819.
[34] L.W. Wang, et al., Anisotropic thermal conductivity and permeability of compacted expanded natural graphite, Appl. Therm. Eng. 30 (13) (2010) 1805–1811.
[35] E.A. Kumar, K.B. Jivrakh, K.S. Babu, Study of ammonia adsorption/desorption characteristics of CaCl2 – expanded natural graphite composite for thermal energy storage, Thermal Science and Engineering Progress 20 (2020) 100752.
[36] A. Grekova, L. Gordeeva, Y. Aristov, Composite sorbents "Li/Ca halogenides inside multi-wall carbon nano-tubes" for thermal energy storage, Sol. Energy Mater. Sol. Cells 155 (2016) 176–183.
[37] W. Li, et al., Characterisation and sorption behaviour of LiOH-LiCl@EG composite sorbents for thermochemical energy storage with controllable thermal upgradeability, Chem. Eng. J. 421 (2021) 129586.
[38] C.A.S. Trindade, et al., Liquid–liquid equilibrium of mixtures of imidazolium-based ionic liquids with propanediols or glycerol, Ind. Eng. Chem. Res. 49 (10) (2010) 4850–4857.

[39] A. Rezk, G. Gediz Ilis, H. Demir, Experimental study on silica gel/ethanol adsorption characteristics for low-grade thermal driven adsorption refrigeration systems, Thermal Science and Engineering Progress 34 (2022) 101429.
[40] A. Pal, et al., Activated carbon and graphene nanoplatelets based novel composite for performance enhancement of adsorption cooling cycle, Energ. Conver. Manage. 180 (2019) 134–148.
[41] H. Banda, et al., Experimental and computational study on utilising graphene oxide for adsorption cooling and water desalination, Appl. Therm. Eng. (2023) 120631.
[42] W. Parker, R. Jenkins, C. Butler, Flash method of determining thermal diffusivity, heat capacity, and thermal conductivity, J. Appl. Sci. 32 (9) (1961) 1679–1684.
[43] Y. Imai, H. Abe, Y. Yoshimura, X-ray diffraction study of ionic liquid based mixtures, J. Phys. Chem. B 113 (7) (2009) 2013–2018.
[44] Z. Li, R. Tao, Performance enhancement of desiccant wheels by adsorption/desorption in stages with type-S isotherm desiccants, Appl. Therm. Eng. 224 (2023) 120068.
[45] M. Thommes, et al., Physisorption of gases, with special reference to the evaluation of surface area and pore size distribution (IUPAC, Technical Report) 87 (9–10) (2015) 1051–1069.
[46] K.H. Chu, et al., The Halsey isotherm for water contaminant adsorption is fake, Sep. Purif. Technol. 313 (2023) 123500.
[47] A.F.M. Cláudio, et al., Extended scale for the hydrogen-bond basicity of ionic liquids, PCCP 16 (14) (2014) 6593–6601.
[48] S.J. Gregg, K.S.W. Sing, H.W. Salzberg, Adsorption surface area and porosity, J. Electrochem. Soc. 114 (11) (1967) p. 279Ca.
[49] R.C. Bansal, M. Goyal, Activated Carbon Adsorption (1st ed.). 2005: CRC Press.
[50] L. Liu, et al., Sorption equilibria, kinetics, and temperature-swing adsorption performance of polyethyleneimine-impregnated silica for post-combustion carbon dioxide capture, Sep. Purif. Technol. 266 (2021) 118582.
[51] T.H. Rupam, et al., Thermodynamic property surfaces for various adsorbent/adsorbate pairs for cooling applications, Int. J. Heat Mass Transf. 144 (2019) 118579.
[52] A. Rezk, et al., Experimental Study on Utilizing Silica Gel with Ethanol and Water for Adsorption Heat Storage. 16 (1) (2023) 444.
[53] A. Jabbari-Hichri, S. Bennici, A. Auroux, Effect of aluminum sulfate addition on the thermal storage performance of mesoporous SBA-15 and MCM-41 materials, Sol. Energy Mater. Sol. Cells 149 (2016) 232–241.
[54] G.T. Whiting, et al., Zeolite–MgCl2 composites as potential long-term heat storage materials: influence of zeolite properties on heats of water sorption, Sol. Energy Mater. Sol. Cells 128 (2014) 289–295.
[55] E. Courbon, et al., Further improvement of the synthesis of silica gel and CaCl2 composites: enhancement of energy storage density and stability over cycles for solar heat storage coupled with space heating applications, Sol. Energy 157 (2017) 532–541.
[56] A. Freni, et al., SAPO-34 coated adsorbent heat exchanger for adsorption chillers, Appl. Therm. Eng. 82 (2015) 1–7.
[57] G. Li, et al., Experimental investigation of energy and exergy performance of short term adsorption heat storage for residential application, Energy 65 (2014) 675–691.